Mechanics of DNA Replication and Transcription Guide the Asymmetric Distribution of RNAPol2 and New Nucleosomes on Replicated Daughter Genomes

Rahima Ziane, Alain Camasses, Marta Radman-Livaja

Mechanics of DNA Replication and Transcription Guide the Asymmetric Distribution of RNAPol2 and New Nucleosomes on Replicated Daughter Genomes

Rahima Ziane[1,2], Alain Camasses[1,2] and Marta Radman-Livaja[1,2*]

[1] *Institut de Génétique Moléculaire de Montpellier, UMR 5535 CNRS, 1919 route de Mende, 34293 Montpellier cedex 5, France;*

[2]*Université de Montpellier, 163 rue Auguste Broussonnet, 34090 Montpellier, France*.

*Corresponding author

Abstract

Replication of the eukaryotic genome occurs in the context of chromatin. Chromatin is commonly thought to carry epigenetic information from one generation to the next, although it is unclear how such information survives the disruptions of nucleosomal architecture occurring during genomic replication. In order to better understand the transmission of gene expression states from one cell generation to the next we have developed a method for following chromatin structure dynamics during replication – ChIP –NChAP – Chromatin Immuno-Precipitation - Nascent Chromatin Avidin Pulldown- which we used to monitor RNAPol2 and new nucleosome binding to newly-replicated daughter genomes in S. Cerevisiae. The strand specificity of our libraries allowed us to uncover the inherently asymmetric distribution of RNAPol2 and H3K56ac-a mark of new histones- on daughter chromatids after replication. Our results show a range of distributions on thousands of genes from symmetric to asymmetric with enrichment shifts from one replicated strand to the other throughout S-phase. We propose a two-step model of chromatin assembly on nascent DNA which provides a mechanistic framework for the regulation of asymmetric segregation of maternal histones, and discuss our model for chromatin assembly in the context of a mechanism for gene expression buffering without a direct role for H3K56ac.

Introduction

All eukaryotic genomic processes happen in the context of chromatin. The smallest repeating subunit of chromatin is the nucleosome: a 147 bp DNA segment wrapped 1.65 turns around a histone octamer core, consisting of one H3/H4 tetramer and two H2A/H2B dimers(Luger et al., 1997). Since architectural features of chromatin limit the accessibility of the DNA substrate to DNA processing enzymes involved in replication, transcription or repair, chromatin -in addition to being a genome packaging system- is the foremost regulatory system for all DNA based processes. Regulatory mechanisms embedded in specific chromatin configurations include: nucleosome positioning along DNA, posttranslational histone modifications, histone variants, and higher order structures such as chromatin loops and topologically associated domains (for reviews see (Bonev and Cavalli, 2016; Jiang and Pugh, 2009; Kornberg and Lorch, 1999; Millar and Grunstein, 2006; Radman-Livaja and Rando, 2010; Rando, 2007; Rando and Ahmad, 2007; Razin et al., 2007)).

Chromatin configuration is perturbed with every round of genome replication, as maternal nucleosomes are disassembled ahead of the replication fork and recycled behind it on the two newly formed daughter chromatids (Foltman et al., 2013). Concomitantly with maternal nucleosome recycling, new histones are assembled on daughter chromatids to restore optimal nucleosome density after genome duplication (for review see (Alabert and Groth, 2012)). Consequently, after every replication event, the cell is faced with two problems: 1. it has to either restore its chromatin configuration on both daughter genomes to its pre-replication state in order to maintain the same transcription program or use the disruption caused by replication as an “opportunity” to modulate chromatin configuration (symmetrically on both genomes or asymmetrically only on one replicated copy) and change the transcription program to launch differentiation or to respond to environmental challenges; 2. it has to globally regulate transcription levels in response to gene copy number doubling after genome replication in G2/M, until cellular division restores single gene copy numbers.

While it is largely accepted that old and new histones bind to both daughter chromatids after replication (Cusick et al., 1984; Gruss et al., 1990), the precise distribution pattern is still not clear: old and new histones could bind completely symmetrically and randomly or in locally asymmetrical segments, thus forming contiguous alternating “patches” of old and new nucleosomes on the same chromatid. The mode of histone distribution has implications for mechanisms of restauration of chromatin states: i.e. how and if potential epigenetic information carried on old nucleosomes is copied to new ones or how asymmetric distribution of gene expression states might be achieved during differentiation. Additionally,

the distribution pattern of old and new histones probably affects the control of transcription after gene copy number doubling. Indeed, Voichek et al., (Voichek et al., 2016) (Voichek et al., 2018) have recently reported that acetylation of K56 on histone H3-a mark of new histones in budding yeast- is needed for transcription buffering. Transcription buffering is a process that maintains constant levels of gene expression throughout S-phase despite gene copy number doubling after replication(Elliott, 1983; Elliott and McLaughlin, 1978).

In order to explore in detail the dynamics of chromatin architecture reestablishment after replication, we developed a high throughput sequencing based technique to map chromatin features on newly replicated DNA – Nascent Chromatin Avidin Pulldown (NChAP)(Vasseur et al., 2016). Using NChAP we determined that nucleosome positioning maturation after replication depends on transcription. We also measured faster nucleosome repositioning on the copy replicated by the leading strand when gene transcription goes in the same direction as the replication fork ("same" orientation genes), while for "opposite" orientation genes repositioning is faster on the lagging strand copy. These two observations- the influence of transcription and genic orientation on nucleosome repositioning rates- led us to hypothesize that at any given time during S-phase only one of the two replicated gene copies is preferentially transcribed. Incidentally, the expression of only one of the two replicated gene copies is one possible mechanism for transcription buffering, the other one being a two- fold decrease in transcription on both gene copies compared to single copy expression in G1.

Using ChIP-NChAP, we were able to show that RNAPol2 and H3K56ac are initially enriched on the leading strand copy, and as chromatin matures after replication, RNAPol2 and H3K56ac enrichments shift to the lagging strand and then back to the leading strand. We also show that H3K56ac has no direct role in RNAPol2 distribution on replicated gene copies and is therefore probably not directly involved in transcription buffering. We propose a two-step chromatin maturation model that explains how the relative rates of replication fork progression and Okazaki fragment maturation direct the asymmetrical distribution of RNAPol2 and new nucleosomes on daughter chromatids.

Results

RNAPol2 ChIP-NChAP

Either mechanism for transcription buffering- preferential transcription of one gene copy or a two-fold decrease in transcription rates on both replicated copies- predicts that the ratio of RNAPol2 occupancy to gene copy number (i.e. DNA content) will decrease approximately two fold compared to the same ratio in G1 after replication of the transcribed

gene. Consequently, we sought to confirm that prediction by measuring the RNAPol2/DNA ratios for all S.Cerevisiae genes during S-phase using two channel DNA microarrays. The HA tagged Rpb3 subunit of RNAPol2, was immuno- precipitated from a synchronized cell population 25min (early S-phase) and 32min (mid early S-phase) after release from α factor induced G1 arrest. The isolated DNA fragments from ChIP and input fractions were then amplified, labeled, mixed and hybridized to whole genome yeast DNA microarrays. As expected, the ratios of RNAPol2 (ChIP DNA)/DNA content (i.e. input DNA) were lower in replicated genes compared to non-replicated genes and the ratios progressively decreased as replication advanced (**Figure 1A**), thus confirming that RNAPol2 density relative to DNA content is indeed reduced after gene copy number doubling.

We next used the RNAPol2 ChIP-NChAP assay to measure the differences in RNAPol2 enrichment between two newly replicated daughter chromatids. The strategy is to grow cells in the presence of the thymidine analogue EdU to label newly replicated DNA strands and then perform ChIP of RNAPol2 (with an HA tagged Rpb3 subunit) followed by isolation of nascent DNA fragments from ChIP-ed DNA using streptavidin pull down after biotinylation of incorporated EdU. The purified nascent DNA is then used to make strand-specific deep-sequencing NChAP libraries as described previously (Vasseur et al., 2016). Watson and Crick strand sequencing reads obtained from these libraries originate from one or the other replicated daughter chromatid, respectively (**Figure 1B**). A comparison between the non-replicated ChIP (RNAPol2 on non-replicated chromatin, rows 8-9 from bottom), ChIP-NChAP (RNAPol2 on replicated chromatin, rows 10-11), and NChAP fractions (replicated chromatin, rows 12-13) from a synchronized population in early S-phase confirms that we are indeed able to isolate replicated DNA specifically bound by RNAPol2 (**Figure 1C**), as only RNAPol2 peaks in replicated regions (see the NChAP fraction) are enriched in the ChIP-NChAP fraction.

Asymmetric Distribution of RNAPol2 on Daughter Chromatids

We next asked how RNAPol2 complexes partition between replicated gene copies. We used the median read density of the coding region of each gene (promoters excluded) from Watson (W) or Crick (C) reads (analyzed separately), as a measure of RNAPol2 occupancy at each gene copy (**Figure 2A**). The heat map in Figure 2A showing median read densities of all yeast genes from ChIP, NChAP and ChIP-NChAP fractions at different time points before and during S-phase (late G1 (2 replicates), early S (54% of the genome still not replicated), early-mid S (21% non-replicated), and mid-early S-phase (10% non-replicated, 2 replicates) confirms the specificity and reproducibility of our assay as RNAPol2 enrichment in the ChIP-NChAP fraction is only detected on replicated genes (compare ChIP-

NChAP and NChAP fractions) and RNAPol2 occupancy correlates well with mRNA abundance.

The scatter plot between median read densities of W and C gene copies from 705 early replicating genes shows that differences in RNAPol2 occupancy between two replicated gene copies are greater on nascent chromatin (the ChIP-NChAP fraction) than on non-replicated chromatin (ChIP fraction). This is not due to experimental artefacts stemming from our strand –specific library construction protocol since differences in W and C read densities are smaller in the nascent chromatin fraction (NChAP fraction) for which we use the same library construction protocol as for the ChIP-NChAP fraction (**Figure 2B**).

Next, we determined the pattern of RNAPol2 distribution between leading and lagging copies relative to genic orientation. Lagging and leading copy annotations for each W and C copy were assigned as described previously (Vasseur et al., 2016): W reads upstream of the closest replication origin (see Figure 1C, Table S1 and Materials and Methods for replication origin mapping) originate from the lagging strand copy, while the complementary C reads are from the leading copy (the opposite is true for reads located downstream of origins). We calculated the ratio of RNAPol2 occupancies between the lagging and the leading gene copy for all 705 early genes, sorted the ratios from lowest to highest, and then divided the set into 7 bins of ~100 genes each. The difference in RNAPol2 density between lagging and leading gene copies appears to be greatest for genes with a low to moderate total RNAPol2 density (i.e. genes with low to moderate gene expression) (**Figure 2C**). This is to be expected if RNAPol2 and transcription factors (TFs) are recycled behind the replication fork and the binding of “new” RNAPol2 complexes and TFs to replicated genes is limited at least in the early period after replication. Smaller quantities of RNAPol2 bound to genes before replication have are more likely to partition asymmetrically between the two replicated gene copies than large amounts of RNAPol2 which are more likely to be distributed symmetrically. Transcription buffering could therefore be a consequence of the constant local concentration of RNAPol2 before and early on after replication: the total transcriptional output from two gene copies after replication is equal to the transcriptional output of one gene copy before replication simply because the locally available RNAPol2 pool is still the same or slightly increased (Figure 1A). The partitioning pattern of the locally available RNAPol2 complexes could then either be unbiased and stochastic or it could have an inherent bias for one over the other copy i.e. a higher tendency to bind to the lagging or the leading copy. As shown in **Figure 2D** RNA pol2 distribution has an inherent bias in a majority of early replicating genes that follows a specific pattern. Genes in the first bin have on average 5.6 times more RNAPol2 on the leading copy than on the lagging and genes in the last bin have 5.8 times more RNAPol2 on the lagging copy. We

calculated the ratio of “same” orientation genes versus “opposite” genes for each bin and normalized it to the “same”/”opposite” ratio of all 705 genes. As predicted from our nucleosome positioning maturation results (Vasseur et al., 2016), “same” gene enrichment is inversely proportional to the nascent RNAPol2 lagging/leading ratio, i.e. “same” genes in early S-phase tend to have more RNAPol2 on the leading copy and “opposite” genes tend to have more RNAPol2 on the lagging copy.

Later on in S-phase, the observed RNAPol2 “polarity” appears to switch and RNAPol2 becomes more abundant on lagging copies when transcription and replication travel in the same direction and on leading copies when they are opposite (**Figure 2E**). RNAPol2 polarity is specific to nascent chromatin as we do not observe significant differences in RNAPol2 occupancies on lagging and leading strands in bulk or non-replicated chromatin (**Supplementary Figure S1**). This “switching” pattern is reproducible as shown in replicate time points in early S-phase (**Supplementary Figure S2)**. However, due to the stochastic nature of replication origin activation the same genes from different early-S phase replicates (even though they appear to be at comparable points in the replication program) are at slightly different points relative to replication fork progression. Consequently RNAPol2 lagging/leading gene ratios do not correlate between different early time point replicates, although later early-S time points correlate better with the mid-early S time-point shown in Fig. 2D (row 4, Fig. S2 B). Nevertheless, a similar RNAPol2 distribution pattern is observed in different replicates: prevalence of RNAPol2 on the leading copy of “same” genes and lagging copy of “opposite” genes in early-S followed by a switch of RNAPol2 enrichment to the lagging copy of “same” genes and the leading copy of “opposite” genes (compare rows 1 and 3 to row 4 in **Fig. S2 B**).

Asymmetric Distribution of H3K56ac on Daughter Chromatids

Acetylation of Lysine 56 on Histone H3 marks newly synthesized histones in yeast (Masumoto et al., 2005). It is consequently enriched at promoters with high H3 turnover rates and on newly replicated DNA (Kaplan et al., 2008). Gene expression microarray experiments with rtt109Δ cells (rtt109 is the H3K56 acetylase) confirmed that transcription buffering after DNA replication is attenuated in the absence of H3K56ac as recently observed (Voichek et al., 2016). Our gene expression analysis also confirmed that EdU addition has no effect on mRNA levels in the rtt109Δ background similar to what we previously observed for wt cells (Vasseur et al., 2016) (**Supplementary Figure S3**). We next checked whether H3K56ac distribution on daughter chromatids correlates with the asymmetric distribution of RNAPol2 described above.

H3K56ac ChIP-NChAP from a synchronized cell population in mid-S-phase (**Figure 3A**) shows that the distribution of this mark of "new" histones indeed correlates with RNAPol2 distribution from mid-early S-phase (**Figure 3B**): RNAPol2 is enriched on the gene copy that also contains more new acetylated histones. Surprisingly, H3K56ac and RNAPol2 lagging/leading ratios do not correlate in early S-phase and even appear to be somewhat anti-correlated (rows 5 and 6 in **Fig. 3B**). H3K56ac does however have a similar distribution pattern between leading "same" and lagging "opposite" genes as RNAPol2 in early S-phase, albeit on different genes (compare rows 3 and 4 from the top in **Fig S2 B**). A recent article has shown that H3K56ac distribution has a slight bias for leading strands around early origins in HU arrested cells (Yu et al., 2018) while an analogous study in mouse ES cells using H4K5Ac as proxy for new histones observed a new histone bias for the lagging strand (Petryk et al., 2018). We performed a similar analysis as in Yu et al. (2018) using the H3K56Ac ChIP-NChAP data from Figure S2 (**Supplementary Figure S4**). Our results provide an explanation for the seemingly contradictory results mentioned above and highlight the importance of performing time courses when attempting to reconstruct dynamic processes. While the earliest time point in our dataset did reproduce the slight H3K56Ac bias for the leading strand, later time points show a switch to the lagging strand (**Supplementary Figure S4A).** Furthermore, as expected from results shown in Figures 3 and S2, the H3K56ac shift from the leading to the lagging strand could be detected at origins with "same" genes only, while H3K56ac was already slightly more enriched on the lagging strand in the earliest time point at origins with only "opposite" genes (**Supplementary Figure S4B).** It therefore appears that the single time points analyzed in the yeast and mouse ES cell studies above have "captured" different steps of the same nucleosome assembly and chromatin maturation process: initial new histone enrichment on the leading strand followed by a shift to the lagging strand.

The lack of correlation between RNAPol2 and H3K56ac lagging/leading enrichment ratios in early S-phase suggests that new nucleosomes and RNAPol2 follow the same order of assembly to daughter chromatids but are independent of each other. The coincidence of H3K56ac and RNAPol2 enrichments later in S-phase would then be a consequence of the convergence of these two independent pathways. Indeed RNAPol2 follows the same asymmetric distribution pattern that appears to switch from one gene copy to the other even in the absence of H3K56ac in rtt109Δ cells (**Figure 4**). What is then the explanation for the apparent loss of transcriptional buffering in rtt109 mutants shown in Figure S3 and by (Voichek et al., 2016; Voichek et al., 2018)? Two rtt109Δ replicates have a narrower distribution of RNAPol2 enrichment per gene, while one replicate has a lower mean RNAPol2 occupancy compared to wt (**Figure 4B**). This suggests that RNAPol2 occupancy is

globally reduced in the absence of H3K56ac as has been observed previously (Rege et al., 2015). This apparent global decrease in RNAPol2 occupancy is corroborated by a duplicate RNA-seq experiment using spike-in normalization with total RNA from *S.pombe*, which shows a ~30% genome wide reduction in mRNA levels in rtt109Δ mutants compared to wt cells (**Supplementary Figure S5**). We therefore conclude that the observed lack of difference in bulk RNAPol2/input-DNA ratios between replicated and non-replicated genes in rtt109 mutants (**Fig. 4C**) that was initially interpreted as a loss of transcription buffering is more likely due, instead, to the global decrease in RNAPol2 occupancy, which "masks" any underlying decrease in RNAPol2 enrichment relative to gene copy number: if the RNAPol2 enrichment in internally normalized bulk ChIP-seq data sets is closer to 0 before replication, it will be harder to detect a relative depletion of RNAPol2 after replication when the gene copy number only doubles, especially in heterogeneous cell population with "noisy" replication synchronicity. The observed increase in mRNA levels from replicated genes relative to non-replicated genes in rtt109Δ cells compared to wt cells is nevertheless still puzzling (**Fig S3**), and could possibly be explained by a transient increase in transcription elongation rates on newly replicated genes specifically in rtt109 mutants (without an increase in RNAPol2 density) as observed by Craig Peterson's group (personal communication), that is likely due to the assembly defect of new nucleosome onto nascent DNA caused by the absence of H3K56ac.

A Two-Step Chromatid "Switching" Model of Nucleosome Assembly and RNAPol2 binding to Daughter Genomes

The results presented above are consistent with two possible models for new nucleosome and RNAPol2 distribution on sister chromatids: 1. a two-step model of H3K56ac/RNAPol2 binding to nascent DNA with initial enrichment on the leading strand followed by a switch to the lagging strand. 2. The two-step cycling model with initial enrichment bias on the leading strand followed by at least one more round of RNApol2 occupancy switching to the lagging strand and then back to the leading strand.

The initial (i.e. immediately after the passage of the replication fork) two steps in nucleosome assembly and RNAPol2 distribution are identical for the two models:

- step 1: The two daughter chromatids are not identical right behind the replication fork. The one that was replicated with leading strand replication is a continuous double stranded DNA helix, while the nascent strand of the other -replicated as the lagging strand- consists of short yet un-ligated Okazaki fragments (~150-200nt in length) bound by complexes involved in Okazaki fragment ligation. Consequently,

maternal nucleosomes, which are recycled behind the fork, compete with new nucleosomes for binding to two structurally very different DNA substrates. Since the local concentration of maternal histones in the proximity of the replication fork is presumably higher than the concentration of new histones, maternal nucleosomes should out-compete new nucleosomes and bind to the leading strand, i.e. the "better" "unobstructed" DNA substrate. Consequently, since the lagging strand is probably bound with factors involved in Okazaki fragment maturation, which probably interfere with transcription, RNAPol2 also binds to the leading strand.

- step 2: After Okazaki fragment maturation new nucleosomes acetylated on H3K56 should populate the lagging strand as the leading strand is already mostly populated with maternal nucleosomes. RNAPol2 also preferentially binds to lagging copies at this stage, although the mechanism for this H3K56Ac independent process is not yet clear. It is possible that RNAPol2 switches to the new nucleosome enriched lagging strand because new nucleosomes tend to be more acetylated than old ones (for eg., new nucleosomes carry H4K5Ac and H4K12Ac(Benson et al., 2006; Sobel et al., 1995)).

In model 1 the second step is the end point: at the end of S-phase all lagging gene copies have more RNAPol2 and more new histones than leading copies. In model 2, there is at least one additional step after which H3K56ac and RNAPol2 are again enriched on leading copies.

The dichotomy in the observed asymmetry of RNAPol2 between genes with the "same" or "opposite" directionalities of transcription and replication is a consequence of the reversed order of replication of promoters and coding regions for "same" and "opposite" genes: promoters are replicated **after** the coding region at **"opposite"** genes while promoters of **"same"** genes are replicated **before** the coding region. Consequently early on in S-phase, when replication timing of early genes in different cells is still reasonably well synchronized, at the time of promoter replication of both "same" and "opposite" genes, the coding regions of "same" genes are still being replicated and Okazaki fragments in the lagging strands have not yet been ligated, while coding regions of "opposite" genes have already undergone replication and Okazaki fragment maturation. Therefore, for any given pair of "opposite" and "same" genes whose promoters replicate at the same time, the step 1 intermediate of the "opposite" gene will assemble before the step 1 intermediate of the "same" gene, resulting in an enrichment of "same" genes on step 1 and "opposite" genes on step 2 in early S-phase.

By mid-early S, however, the asymmetries in RNAPol2 and H3K56ac distributions are not detectable or greatly diminished on genes that replicated the earliest because the

signal is by now a mixture of step 1 and step 2 structures due to imperfect synchronicity of replication forks in different cells. Mid-early replicating genes in mid-early S-phase, on the other hand, are mostly on step 2 or on step 1 if they are “same” or “opposite” genes, respectively. The observed pattern reversal is possibly due to delayed replication of “opposite” genes relative to “same” genes later in S-phase. The delay in the replication of “opposite” genes relative to “same” genes, may be a consequence of a progressive slowing down of replication forks traveling through “opposite” genes. This hypothesis is supported by two observations. First: the difference in replication timing between “opposite” and “same” genes increases with S-phase progression (**Supplementary Figure S6A**). By mid-S-phase (genes replicating 45-55min after release from arrest) “opposite” genes are replicated on average 1.5min later than “same” genes, meaning that at the time of replication of promoters from “opposite” genes, replication forks have already moved 1.5kb to 3kb away from promoters of “same” genes if we assume an average fork speed of 1 to 2 kb/min (Yang et al., 2010). Second: genes of the same genic orientation tend to be replicated in succession by the same replication fork (**Supplementary Figure S6B**). Consequently, a replication fork passing through an array of “opposite” genes is more likely to slow down compared to a fork replicating “same” genes, presumably because of successive and disruptive “head on” encounters with the transcription machinery in “opposite” gene clusters.

We can distinguish between the two models if we perform an EdU pulse chase experiment in asynchronous cell populations (**Figure 5A**). The pulse-chase experiment in asynchronous cell population allows us to follow chromatin maturation and RNAPol2 dynamics at all genomic loci independently of replication timing. We have chosen to look at H3K56ac and RNAPol2 distribution on replicated gene copies at 7min and 15min after the initial 1min EdU pulse because in our culture condition EdU stops being incorporated into DNA in the cell population as a whole at 7min after the pulse and at 15min replication forks have moved at least 7-14kbp from the EdU labeled loci, and we assume that chromatin maturation should be in the last stages of the process at all labeled loci by this time. As illustrated in **Figure 5B,** the predicted shape of the scatter plot of nascent H3K56ac/RNAPol2 lagging strand enrichment (lagging/leading) at 7 or 15 min after EdU addition versus the change in lagging strand enrichment from 7min to 15min will be different depending on the model. In the first model we expect that, genes with a H3K56ac or an RNAPol2 enrichment on the leading strand at the 7min time point followed by a H3K56ac/RNAPol2 switch to the lagging strand at the 15min point would predominantly be co-directional or “same” genes, while on “opposite” genes H3K56Ac/RNAPol2 should already be enriched on the lagging strand at the 7min point and stay there at the 15min point. On the other hand, model 2 predicts that H3K56ac/RNAPol2 should be enriched on

the leading strand at 7min and switch to the lagging strand at 15min on “same” genes, and vice versa on “opposite” genes. The results of a duplicate EdU pulse chase experiment fit model 2 better (**Figure 5 C-E**). The pattern of RNAPol2 distribution relative to gene orientation follows our prediction for model 2 (Figure 5D). H3K56ac enrichment dynamics appear however to go in the opposite direction: from leading to lagging on “opposite” genes and from lagging to leading on “same” genes (Figure 5E). The occupancy shifts shown in Figure 5D-E, are also confirmed with average RNAPol2 and H3K56ac density profiles of tss aligned gene groups ordered according to the magnitude and direction of the change in enrichment asymmetry between the lagging and leading copies during the time course (Figure 5 F-G). The observed asymmetries are specific for nascent chromatin as leading and lagging gene profiles from all gene groups in bulk chromatin are indistinguishable from each other. It has been previously shown that rapid nucleosome turnover at promoters persists throughout S-phase (Kaplan et al., 2008). H3K56ac peaks at the tss and the 3’end of genes (most yeast genes are 2 to 3kb in length) in nascent chromatin profiles now confirm that nucleosome turnover at gene extremities resumes shortly after the passage of the replication fork on both newly replicated gene copies. This observation argues against the possibility that transcription buffering is caused by an H3K56ac dependent inhibition of nucleosome turnover at promoters (which is thought to stimulate transcription) that would also be specific for replicated chromatin.

We propose the following chain of events that is consistent with our results: For “same” genes, H3K56ac is initially enriched on the leading strand because the lagging strand is not chromatinized during Okazaki fragment maturation (step 1, not captured in the experiment). 7min after the EdU pulse, H3K56ac enrichment switches to the lagging strand after Okazaki fragments have matured thus allowing the assembly of new nucleosomes (step 2) and 15min after the pulse partial deacetylation of H3K56ac causes an apparent switch of H3K56ac to the leading strand (step 3). The lagging strand is possibly partially deacetylated before the leading strand because it has a higher concentration of H3K56ac and is hence a higher affinity substrate for hst3/4 deacetylases (that are specific for H3K56ac (Celic et al., 2006). “Opposite” genes are already on step 3 at the 7min point and at the 15min point deacetylation in the gene body of leading copies and H3K56ac levels are now almost identical on the leading and lagging copies (**Figure 5G**). RNAPol2 binding lags behind new nucleosome assembly, so 7min after the EdU pulse RNAPol2 is on the leading copy (step 1) or on the lagging copy (step 2) for same or opposite genes, respectively. At the 15min point RNAPol2 switches to the lagging copy for same genes (step 2) or leading copy (step 3) for opposite genes.

Discussion

Our strand specific ChIP-NChAP technique enabled us to measure the dynamics of the genome wide asymmetrical distribution of newly synthesized nucleosomes and RNAPol2 complexes on the two replicated daughter chromatids. Our results are consistent with a two-step model of chromatin structure re-establishment after DNA replication that provides a mechanistic framework for transcription buffering and also explains how gene expression states and chromatin configuration are maintained or could potentially change from one cell generation to the next (**Figure 6A**).

Since our results do not support a direct role of H3K56ac in transcription buffering as previously suggested (Voichek et al., 2016; Voichek et al., 2018), we propose that transcription buffering stems from the limiting local concentration of transcription factors and RNAPol2 shortly after replication. Transcription resumes at “half capacity” shortly after replication using mostly the locally available “recycled” TFs and RNAPol2 because it takes some time to build up sufficient quantities of new additional transcription factors and RNAPol2 complexes that are necessary to double the transcriptional output using two replicated gene copies. Consequently, transcription buffering, i.e. delaying until G2 the two-fold increase of transcriptional output that is expected after gene copy number doubling, would essentially be the length of time necessary to accumulate sufficient quantities of transcription machinery components.

The apparent “recycling” of RNAPol2 and the distribution of new nucleosomes to replicated daughter chromatids is however not random. We hypothesize that the initial asymmetric enrichment of new nucleosomes and RNAPol2 on the leading strand is a consequence of the slower rate of Okazaki fragment maturation relative to replication fork speed. Immediately after the passage of the fork maternal nucleosomes and some new nucleosomes are preferentially assembled on the leading strand because the lagging strand is still in the process of Okazaki fragment ligation and is therefore presumably not a good substrate for nucleosome assembly. H3K56ac is consequently initially enriched on the leading strand because there are relatively fewer nucleosomes on the lagging strand (step 1). The majority of new nucleosomes bind to the lagging strands later on when Okazaki fragments are mature because the leading strand is by then already mostly occupied by maternal nucleosomes (step 2). The subsequent switching of H3K56ac enrichment from the lagging to the leading strand (step 3) is somewhat more puzzling and could be explained by a partial deacetylation of first the lagging gene copy followed by the leading copy. This explanation however implies that there is a low level of deacetylase activity that occurs throughout S-phase, which remains to be tested. RNAPol2 binding to replicated genes follows the same steps as new nucleosome binding although with somewhat of a lag behind nucleosome assembly. Since H3K56ac and RNAPol2 distribution on replicated DNA do not

correlate in the early time points after the passage of the replication fork it is still not clear why the enrichment in RNAPol2 occupancy switches from the leading to the lagging strand and then back again to the leading gene copy. While H3K56ac does indeed stimulate transcription as shown by spike-in normalized RNA-seq experiments (**Supplementary Figure S3**), the asymmetric binding and apparent switching of RNAPol2 from the leading to the lagging copy is independent of rtt109 mediated H3K56 acetylation. RNAPol2 may still switch to the gene copy enriched for new nucleosomes due to their generally hyper acetylated state (Ge et al., 2013; Jackson et al., 1976; Sobel et al., 1995), although further experiments are needed to test this assumption.

After global H3K56 deacetylation in late S (Celic et al., 2006) nucleosomes from the two daughter copies are indistinguishable: since transcription has been alternating between the two replicated copies throughout S-phase. Both copies should therefore carry the H3K4me3, H3K36me3 and H3K79me3 marks characteristic of transcribed genes. Consequently the mother and the daughter cells should inherit gene copies with identical chromatin configurations (**Figure 6B**).

The prediction of our model is that daughter chromatids should be “decorated” with contiguous alternating “patches” of old and new nucleosomes as illustrated in **Figure 6C** (middle panel), due to the even distribution of replication origins along yeast chromosomes and the bi-directionality of replication forks. According to our model a decrease in replication fork speed relative to the rate of Okazaki fragment maturation, such that Okazaki fragments are ligated while the fork is still at a relatively short distance from the newly synthesized Okazaki fragments, should reduce the bias of old histones for the leading strand and result in a more random and symmetrical distribution as shown in the left panel of **Figure 6C**. On the other hand, complete asymmetrical segregation of old and new histones could potentially occur if replication fork barriers were introduced on the same side of all or most replication origins on the same chromosome, thus making replication unidirectional throughout the chromosome (right panel, **Figure 6C**).

Alternatively, new histones could be enriched on the lagging strand by a nucleosome assembly mechanism specific for new histones. The DNA polymerase processivity clamp PCNA is enriched on the lagging strand ((Yu et al., 2014),reviewed in (Choe and Moldovan, 2017)). Since PCNA recruits the Chromatin Assembly Factor 1 (CAF1) to the replication fork (Gerard et al., 2006) and CAF1 is responsible for the deposition of new H3-H4 tetramers on replicated DNA (Kaufman et al., 1995; Li et al., 2008; Mattiroli et al., 2017; Sauer et al., 2017; Yang et al., 2016), the expectation is that new histones will be enriched on the lagging copy as predicted by our model and supported by our data.

A mechanism for nucleosome distribution bias that relies on competition between new and old nucleosomes for binding to newly replicated DNA as a function of varying Okazaki fragment maturation rates relative to fork speed, is however more flexible than a system that specializes in the preferential deposition of new histones on lagging strands such as the one based on PCNA/CAF1 mentioned above. With the first system, cells could achieve varying degrees of segregation bias of old nucleosomes at different genomic loci by locally modulating replication fork speeds and/or Okazaki fragment ligation rates thus shifting between symmetric segregation and "patched" asymmetric segregation in a locus dependent manner (**Figure 6C**). With a specialized nucleosome deposition system, the cell could only vary which segments on any given chromatid are preferentially covered by new or old nucleosomes by activating different replication origins or replication fork barriers and thereby determining where lagging and leading replication will take place. Symmetric distribution could never result from such a system unless there is an additional mechanism in place that ensures symmetric segregation of old histones and also promotes binding of new histones to the leading as well as the lagging strands. The Mcm2 subunit of the replication fork helicase Mcm2-7 has recently been implicated in the recycling of old nucleosomes behind the fork (Foltman et al., 2013). Since an Mcm2 mutation that impairs the interaction between histone H3 and Mcm2 enhances the bias of old nucleosomes for the leading strand, two studies have argued that Mcm2 promotes re-assembly of old nucleosomes onto the lagging strand in order to counteract the "natural" tendency of old nucleosomes to re-bind to the leading strand (Gan et al., 2018; Petryk et al., 2018). In light of our results showing locus specific dynamic shifts in the asymmetrical distribution of histones and RNAPol2 depending on the timing of replication of each gene in the population, and given the stochastic nature of DNA replication timing and the impossibility to fix different cell populations at exactly the same time of genome replication (especially in early S-phase), it is probable that histone distributions observed in one (Petryk et al., 2018) or at most two time points (Gan et al., 2018) do not represent the same chromatin maturation time point in wt and mutant cells and are therefore not comparable. With that caveat in mind, the interpretation of the Mcm2 mutant data presented in these studies still begs the questions: what is the molecular mechanism that "naturally" directs old nucleosomes to the leading strand and which factor recycles histones behind the fork when Mcm2 is impaired? The model we propose on the other hand does not require specialized systems for old or new nucleosome deposition that are specific for the leading or the lagging strand. The effect of the Mcm2 mutation mentioned above could instead be explained if the mutation increases fork velocity thereby leaving longer stretches of non-ligated Okazaki fragments behind and thus favoring old nucleosome binding to the leading strand. Likewise, enhanced old histone deposition on the lagging strand observed in mutants of the subunits of the leading strand DNA polymerase ε Dpb3/4

(Yu et al., 2018) may have been caused by slowing down of the replication fork that gave time to Okazaki fragment maturation to “catch up”, thus facilitating old histone binding to the lagging strand.

In order for chromatin features to be truly epigenetic, they have to be accurately transmitted after cell division and they have to be instructive of the transcription state at their genomic location. It has recently been shown that gene “silencing” histone marks such as H3K27me3 and H3K9me3 are indeed inheritable (Coleman and Struhl, 2017; Laprell et al., 2017; Wang and Moazed, 2017). Thus, if such specific local chromatin configurations have to be inherited in only one daughter cell after cell division (either mother cell or bud for yeast; either stem cell or differentiating cell for multicellular organisms) the bias in maternal nucleosome segregation could be enhanced at those loci by increasing fork speed or delaying Okazaki fragment maturation or by initiating unidirectional replication from nearby origins. Thus, our model provides a mechanistic blueprint for asymmetric nucleosome segregation after genome replication, for even the most extreme case of nucleosome segregation bias like the one recorded in Drosophila male germline stem cells (Tran et al., 2012; Xie et al., 2015), where the full complement of old nucleosomes is retained in the stem cell. As illustrated in Figure 6C, we speculate that such complete asymmetric maternal nucleosome segregation could be achieved by replication with unidirectional forks throughout the chromosome.

Clearly, any locally asymmetrical nucleosome segregation would have to be coordinated with chromatid segregation during mitosis so that all the local chromatin configurations relevant for a specific cellular phenotype are regrouped in the same cell. One of the future challenges in understanding asymmetric cell divisions is therefore to decipher the molecular mechanism for coordinated co-segregation of genes with the relevant chromatin configurations that are dispersed throughout the chromosome and not necessarily contiguous.

Materials and Methods

Yeast Strains

All yeast strains have a W303 background and are listed in Table S3. The wt strain RZ71 containing the HA tagged Rpb3 RNAPol2 subunit was obtained from a cross between ES3086 (courtesy of E. Schwob) and YMTK2567 (courtesy of Traci Lee). The Rtt109Δ strain RZ72 (Figure 5) was obtained by crossing RZ71 with ZGY929 (courtesy of Z.Zhang). The Rtt109Δ strain RZ23 (Figure S3) was obtained from a cross between ES3086 and ZGY954 (courtesy of Z. Zhang). The Rtt109Δ (RZ72 and RZ23) and hst3,4ΔΔ (PKY4220, courtesy of

Paul Kaufman, Figure S5) strains have been additionally validated by anti H3K56ac western blotting of bulk mid-log cell extracts (data not shown).

Cell Culture

H3K56ac ChIP-NChAP (Figure 3): Cells were grown overnight at 30°C in 500ml Synthetic Complete- URA + Dextrose (SCD-URA) media to OD 0.3. After 3.75hrs at 30°C with α factor (0.15µg/ml), cells were pelleted and transferred into preheated and premixed SCD-URA+ 10µM EdU(Carbosynth), with freshly added 20µg/ml pronase (Sigma). The culture was fixed with 1% formaldehyde after 24min (early S) or 30min (mid S) incubation at 30°C, incubated for 30min at 30°C and quenched with 125mM Glycine. Cell pellets were then washed with water and flash frozen in liquid nitrogen and kept at -80°C until further processing.

Rpb3-HA and H3K56ac time course ChIP-NChAP, synchronized (Figures 1, 2, 4, S1, S2):

Cells were grown overnight at 30°C in SCD-URA. The culture was diluted to OD_{600} ~0.3 the next morning and grown to OD_{600} ~0.65 and re-diluted to OD_{600} ~0.3 (total final volume 10L) in fresh media. The culture was synchronized with the addition of 0.15 µg/ml α factor for 3h30min at 30°C. Cells were released from arrest as above in preheated (SCD-URA)+10µM EdU + 20µg/ml pronase. At 20, 22, 24, 25 (or 26), or 32 min after release, cells (2.5L per time point) were fixed with 1% (w/v) formaldehyde for 15 min at 30°C followed by 5 min of quenching in 125 mM Glycine. Cell pellets were then washed with PBS and flash frozen in liquid nitrogen and kept at -80°C until further processing.

Rpb3-HA and H3K56ac time course ChIP-NChAP, asynchronous, EdU-Thymidine pulse chase (Figure 5):

Mid-log cells (grown o/n in SCD-URA at 30°C, OD_{600} ~0.68) were treated with 10µM EdU for 1min by mixing equal volumes of culture and preheated (30°C) premixed media containing 20µM EdU. EdU incorporation was stopped with the addition of Thymidine (Acros Organics , previously mixed into preheated SCD-URA media) to a final concentration of 10mM (1000 fold excess) to the culture. The culture was divided into two flasks and the ½ cultures were fixed with formaldehyde 7 or 15 minutes after EdU addition. H3K56Ac and RNAPol2 ChIP-NChAP with sonicated chromatin were then performed in parallel.

MNase digestion

H3K56ac ChIP-NChAP (Figure 3):700µl 0.5mm glass beads were added to frozen cell pellets (equivalent of 100ml cell cultures OD=0.5), re-suspended in 700µl cell breaking buffer (20% glycerol 100mM Tris-HCl 7.5). Cells were then spheroplasted by bead beating in the Bullet Blender (Next Advance) for 4x3min at strength 8 in the cold room. Spheroplasts

were recovered by puncturing the cap of the tube and spinning into 5ml eppendorf at 1000rpm for 3 min. Cells were then centrifuged 5min at maximum speed in a micro centrifuge and the clear top layer was discarded, each pellet was re suspended in 600ul NP buffer (50mM NaCl, 10mM Tris-HCl pH 7.4, 5mM $MgCl_2$, 1mM $CaCl_2$,0.075% NP-40, 0.5mM sperimidine, 1mM βME).The amount of MNase (Worthington Biochemical) was adjusted to the cell density in each tube in order to obtain 80-90% mononucleosomal sized fragments after 20min incubation at 37°C. The reaction was stopped with 10mM EDTA and used for H3K56ac ChIP as described below.

Chromatin Sonication

Cross-linked frozen cell pellets were re-suspended in 1.5 ml Lysis buffer (50mM NaCl, 10mM Tris 7.4, 0.075%NP-40, 1mM EDTA, 0.1%-0.5%SDS (optional), 1mM PMSF and 1xEDTA-free protease inhibitor cocktail (Roche)). The suspension was then split into aliquots with ~10^9 cells each. Zirconium Sillicate beads (400 µl ,0.5 mm) were then added to each aliquot and cells were mechanically disrupted using a bullet blender (Next Advance) for 4 times x3 min (intensity 8). Zirconium beads were removed from the cell lysate by centrifugation and the entire cell lysate was subject to sonication using the Bioruptor-Pico (Diagenode) for 3x10 cycles of 30 seconds *ON*/OFF each resulting in a final median size of chromatin fragments of 200 bp. Cellular debris was then removed by centrifugation and 2% of the total supernatant volume was kept for the input and NChAP fractions.

Chromatin Immunoprecipitation (ChIP)

H3K56ac (Figure 3): All steps were done at 4°C unless otherwise indicated. For each aliquot, Buffer L (50 mM Hepes-KOH pH 7.5, 140 mM NaCl, 1 mM EDTA, 1% Triton X-100, 0.1% sodium deoxycholate) components were added from concentrated stocks (10-20X) for a total volume of 0.8 ml per aliquot. Each aliquot was rotated for 1 hour with 100 µl 50% Sepharose Protein A Fast-Flow bead slurry (IPA400HC, Repligen) previously equilibrated in Buffer L. The beads were pelleted at 3000 X g for 30sec, and approximately 100 µl of the supernatant was set aside for the input sample. With the remainder, antibodies were added to each aliquot (equivalent to 100 ml of cell culture): 6µl anti- H3K56ac for the mid-S time point (Merck-Millipore, 07-677-IS (lot# 266732) or 10 µl anti- H3K56ac for the early-S time point (Active Motif, 3928 (lot# 14013003). Immunoprecipitation, washing, protein degradation, and DNA isolation were performed as previously described (Liu et al., 2003). Purified DNA was treated with RNAse A (Qiagen) and CIP (NEB) and purified once more with Phenol-Chloroform. Fragments shorter than 100bp were removed with homemade MagNA beads (SeraMag Speed beads, Thermo Scientific,(Rohland and Reich, 2012)), and

purified fragments were used for NGS library construction (Input, ChIP) or biotin conjugation and subsequent NGS library construction (NChAP, ChIP-NChAP).

Rpb3-HA and H3K56ac (Figs. 1,2,4,5, S1 and S2):

Sonicated chromatin was precleared using Protein A agarose beads (Repligen) for 1 h at 4°C on the rotating wheel. The sonicated material was then pooled together and distributed into 500µL aliquots (equivalent of $7*10^8$ cells per aliquot) and 25 µl of Protein G magnetic beads (Life Technologies-Invitrogen) pre-bound with 6 µg or 3 µg of anti-HA (ab9110, abcam) or anti-H3K56ac (Active motif), respectively, was added to each tube. Aliquots were then incubated with rotation at 4°C overnight. The beads were then washed two times with cold buffer L (50 mM HEPES-KOH, pH 7.5, 140 mM NaCl, 1 mM EDTA, 1% Triton X-100, 0.1% Na-deoxycholate), once with cold Buffer W1 (Buffer L with 500mM NaCl), twice with cold Buffer W2 (10 mM Tris-HCl at pH 8.0, 250 mM LiCl, 0.5% NP-40, 0.5% sodium deoxycholate, 1 mM EDTA), and once with cold TE buffer (10 mM Tris-HCl at pH 8.0, 1 mM EDTA). Chromatin was eluted in 2x125 µl elution buffer (10 mM Tris-HCl at pH 8.0, 1 mM EDTA, 1% SDS, 150 mM NaCl, 5 mM DTT) by incubation for 10 min at 65°C. The eluates and reserved input samples were treated with RNase A (Qiagen) for 1h in 37°C and proteins were then digested with Proteinase K (Euromedex, final concentration 0.4 mg/ml) for 2h at 37°C and the temperature was then shifted to 65°C for cross-link reversal overnight. DNA was then purified with the QIAquick PCR purification kit (QIAGEN) except for the early S-phase time point (54% non-replicated) from Fig 1C and Fig 2 that was purified by Phenol Chloroform extraction to keep fragments smaller than 100bp, which increases the resolution for mapping of replication origins.

Biotin conjugation to EdU with the Click reaction

10µl DNA solution was mixed with 10µl biotin azide (quanta biosystems) solution in DMSO/tBuOH(3:1). For each pmole of DNA, we added 1mM biotin azide solution (for example for 20pmoles of DNA in 10µl, 10µl 20mM biotin azide were added). 10µl CuBr solution (10mM CuBr (from freshly made stock), 10mM TBTA (Eurogentec), 10mM Ascorbic acid (from freshly made stock) in DMSO/tBuOH 3:1) were then added to the DNA-biotin azide mix and the reaction was shaken for 2hrs at 37°C. 300µl 10mMTris-HCl pH7.5, 8µl 0.25% linearized acrylamide solution, 33µl 3M Sodium Acetate pH5 and 1ml 100% cold EtOH were then added to the Click reaction and DNA was precipitated at -20°C overnight.

Illumina Sequencing Library Construction

ChIP-NChAP and NChAP libraries: Biotinylated DNA pellets were re suspended in 25µl TNE0.2 buffer (200mM NaCl, 10mMTris-HCl 7.5, 1mM EDTA) and mixed with 25µl

Streptavidin coated magnetic beads (NEB, pre washed in TNE0.2 and blocked with 100µg/ml salmon sperm DNA). The DNA and bead mixture was shaken for 30min at RT, and beads were washed 2x with 0.25ml TNE0.2 buffer and re suspend in 35µl 10mM Tris-HCl pH8. All the subsequent steps were done with DNA attached to the beads. DNA fragments were blunt ended and phosphorylated with the Epicentre End-it-Repair kit (1X buffer, 0.25mM dNTPs,1mM ATP, 1µl Enzyme mix in a 50µl reaction) for 1hr at RT. Beads were washed 2x with TNE0.2 and re suspended in 43µl 10mM Tris-HCl pH8. Adenosine nucleotide overhangs were added using Epicentre exo- Klenow for 45min at RT (with 0.2mM dATP) followed by two TNE0.2 washes and re suspension in 15µl 10mM Tris-HCl pH8. Illumina Genome sequencing adaptors with in line barcodes (

PE1-NNNNN: PhosNNNNNAGATCGGAAGAGCGGTTCAGCAGGAATGCCGAG

PE2-NNNNN: ACACTCTTTCCCTACACGACGCTCTTCCGATCTNNNNNT

, NNNNN indicates the position of the 5bp barcode, (IDT)) were then ligated over night at 16°C using the Epicentre Fast-Link ligation kit. The ligation reaction was washed 2x with TNE0.2 and beads were re suspended in 20µl water. DNA was then subjected to a primer extension reaction with dUTP to separate the nascent strand from its complement (1X NEB buffer2, 0.1µg/µl 5'phosphorylated random hexamers (IDT), 1.72 µM Illumina PE primer 2.0 (IDT), 0.6 mM dNTPs (dUTP instead of dTTP) and 2U/µl Klenow 5NEB). DNA was denatured and annealed to the primers prior to enzyme addition and the reaction was incubated 1.5 hrs at 37°C. Beads were washed 4x and re suspended in 20µL water. The dUTP containing strand was degraded with USER enzyme (NEB) and beads were re suspended after washing in 20µl 10mM Tris-HCl pH8.

The remaining nascent DNA strand was amplified with the Phusion enzyme (NEB) for 18 PCR cycles with Illumina PE1 (AATGATACGGCGACCACCGAGATCTACACTCTTTCCCTACACGACGCTCTTCCGATCT) and PE2 (CAAGCAGAAGACGGCATACGAGATCGGTCTCGGCATTCCTGCTGAACCGCTCTTCCGATCT) primers (IDT). Only 2µl of the bead suspension was added to the 50µl PCR mix. Amplified libraries were purified using MagNA beads (SeraMag Speed beads, Thermo Scientific,(Rohland and Reich, 2012)) and fragment size and library concentration were determined from a Bioanalyzer (Agilent) scan and Qubit fluorimetry measurements, respectively.

Input and ChIP libraries:

Libraries were constructed as above from the blunt ending step. DNA fragments were blunt ended and phosphorylated with the Epicentre End-it-Repair kit. Adenosine nucleotide overhangs were added using Epicentre exo- Klenow. Illumina Genome sequencing adaptors with in line barcodes (above) were then ligated over night at 16°C using the

Epicentre Fast-Link ligation kit. Ligated fragments were amplified as above using the Phusion enzyme. Reactions were cleaned between each step using MagNa beads.

Libraries for input and ChIP (H3K56ac and Rpb3-HA) fractions from replicates 1 and 2 (52%, 45% and 38% non-replicated) from Fig. S2 and for input and Rpb3-HA ChIP from rtt109Δ replicates (17% and 10% non-replicated) from Fig. 4 were prepared using the TrueSeq V2 LT Sample prep kit (Illumina).

Illumina Sequencing

Libraries were mixed in equimolar amounts (10 to 15 libraries per pool) and library pools were sequenced on a HiSeq 2000 (2x75bp) (Illumina) at the CNAG, Barcelona, Spain.

RNAseq with spike-in control (Figure S5)

Exponentially growing S.cerevisiae and S. pombe (strain FY2319, courtesy of S. Forsburg) cells were flash frozen in liquid N2 and total RNA was isolated from frozen cell pellets with Trizol. Frozen cell pellets were re-suspended directly in Trizol and bead beated in the Bullet Blender (Next Advance) as above. RNA was then purified and DNAseI treated with the RNAeasy Column purification kit (Qiagen). Extracted total RNA amounts were measured on the Qubit and Nanodrop and the quality was checked with a Bioanalyzer scan (Agilent). Each S.cerevisiae total RNA extract was mixed with the S.pombe total RNA extract at a mass ratio of 10:1. The mixed RNA samples were then used for NGS library preparation using the Illumina TruSeq Stranded mRNA kit according to the manufacturer's protocol.

ChIP DNA Microarray hybridization (Figure 1A)

ChIPped DNA and their corresponding input samples were amplified, with a starting amount of up to 30 ng, using the DNA linear amplification method described previously (Liu et al., 2005; Liu et al., 2003). 2.5 µg of aRNA from each sample produced from the linear amplification was transformed into cDNA by reverse transcription in the presence of amino-allyl dUTP. The resulting cDNA was dye-coupled with Cy5 or Cy3 NHS-esters and purified as described previously (Liu et al., 2005).

Labeled probes (a mixture of Cy5 labeled input and Cy3 labeled ChIPed material or their corresponding dye flips) were hybridized onto an Agilent yeast 4x44 whole genome array. Images were scanned at 5µm with the InnoScan 710 MicroArray scanner (Innopsys) and processed with the Mapix software. Data was normalized by dividing the Cy3/Cy5 (or Cy5/Cy3 ratio for the dye flip) ratio for each probe with the average Cy3/Cy5 ratio for the whole array. The average of the pair of normalized ratios from the dye flip technical

replicates was used in the final analysis. The GEO accession number for the microarray data is

Gene Expression Microarray hybridization (Figure S3)

Rtt109Δ cells were arrested in G1 with α factor as above. Genomic DNA was isolated from G1 arrested flash frozen cell pellets with Phenol/Chloroform, and sonicated with the Bioruptor Pico cup sonicator (200µl at 200ng/ µl, 30"ON 30"OFF at 4°C). Cells were released into S phase in media with or without 10µM EdU, as above. 50ml aliquots were flash frozen in liquid nitrogen 32 and 40min after release, for RNA isolation.

Total RNA was isolated from frozen cell pellets with Trizol. Frozen cell pellets were re-suspended directly in Trizol and bead beated in the Bullet Blender (Next Advance) as above. RNA was then purified and DNAseI treated with the RNAeasy Column purification kit (Qiagen).

We used ~30 µg of total RNA for each expression array. RNA was reverse transcribed using oligodTs(0.15µg/µl final) as primers. Reactions (0.5mM dNTP (N=A,G,C),0.2mMdTTP and 0.3mM amino-allyl dUTP (SIGMA),6µg/ml Actinomycine D (SIGMA), 10mMDTT, 1XFS buffer and 10U/µl Superscript III (Life technologies)) were incubated at 50°C for 2hrs. RNA was then degraded with NaOH at 65°C (10µl 1N NaOH and 10µl 0.5M EDTA into 30µl reactions), the solution was neutralized with HEPES pH=7.5 (25µl 1M stock) and the buffer was exchanged for water in Amicon30 centricon spin columns. The resulting cDNA was dye-coupled with Cy5 or Cy3 NHS-esters and purified as described previously (Liu et al., 2005).

The Cy5 or Cy3 labeled cDNA was mixed with Cy3 or Cy5 labeled genomic DNA, respectively (genomic DNA labeling: 2µg (quantified in the Qubit fluorimeter) PV1 genomic DNA from the G1 cell cycle phase in Klenow NEB buffer, 0.3 µg/µl random hexamers, 0.12 mM dNTP (N=A,G,T),0.06mM dCTP and 0.06mM Cy5 or Cy3 conjugated dCTP (GE healthcare), and 1U/µl Klenow enzyme (NEB); incubated 2hrs at 37°C and cleaned up in Amicon-30 spin columns). Labelling efficiency of cDNA and genomic DNA was verified with the Nanodrop spectrophotometer. The labeled mixture was combined with hybridization buffer, following the Agilent microarray hybridization protocol and hybridized to Agilent 8x15K yeast Gene Expression arrays at 65°C for 16hrs. Images were scanned at 5µm with the InnoScan 710 MicroArray scanner (Innopsys) and processed with the Mapix software. Data was normalized by dividing the Cy5/Cy3 ratio for each probe with the average Cy5/Cy3 ratio for the whole array. The GEO accession number for the microarray data is

Cytometry

Cells preparation and flow cytometry were performed as described previously (Talarek et al., 2015; Vasseur et al., 2016).

Data Analysis

All analysis was done using in house Perl and R scripts available upon request.

ChIP, ChIP-NChAP, NChAP:

Sequences were aligned to S. Cerevisiae genome using BLAT (Kent Informatics, http://hgdownload.soe.ucsc.edu/admin/). We kept reads that had at least one uniquely aligned 100% match in the paired end pair. Read count distribution was determined in 1bp windows and then normalized to 1 by dividing each base pair count with the genome-wide average base-pair count. Forward and reverse reads were treated separately.

The repetitive regions map was constructed by "BLATing" all the possible 70 bp sequences of the yeast genome and parsing all the unique 70bp sequences. All the base coordinates that were not in those unique sequences were considered repetitive.

Normalized read densities for all genes were aligned by the transcription start site (Xu et al., 2009) and median read densities for each coding region (from the tss to the transcription termination site) were determined for all datasets. Median read densities from ChIP and NChAP (nascent chromatin) fractions were normalized to the median from their corresponding input (sonicated or MNAse digested chromatin) and medians from ChIP-NChAP fractions were then normalized to the corresponding input normalized ChIP fraction.

Replicated genome fraction:

Normalized read counts, binned in 400bp windows over the whole genome, from NChAP fractions (and the H3K56ac mid S ChIP fraction, Fig. 3) in each chromosome were divided by the maximum read count for that chromosome to obtain population read densities (i.e. the fraction of the cell population in which each 400bp genome segment has been replicated). We then determined the distribution of these read densities into 100 bins from 1% to 100%. The non-replicated fraction was the genome fraction with read densities between 0 and 1%.

Replication origins mapping:

Origins were mapped from the nascent chromatin fraction in the early S-phase dataset from Figure 1C and Figure 2 (54% non-replicated). The resolution for origin centers was higher in this dataset because small fragments (<100bp) were not removed from this fraction (see the Chromatin Immunoprecipitation (ChIP) section). We identified local peaks within Replication Associated Domains (replicated regions around known origins of replication) on every chromosome (Table S1). We then looked for ACS consensus sequences (Nieduszynski et al., 2007) within +-200bp of each identified peak and kept the ACS sequence closest to the peak (Table S2). Peaks without ACS sequences were eliminated from further analysis.

RNA-seq normalized to S.Pombe spike-in:

S.Cerevisiae and S.pombe reads were aligned to their respective genomes using BLAT and the read density distribution was determined for each species in each dataset separately. The average S.pombe genomic read density per bp (F and R reads were processed together) was determined for each dataset. For spike-in normalization, S.Cerevisiae read densities per bp were then divided with the corresponding S.pombe average genomic read density. For internal normalization S.Cerevisiae read densities were divided with its average genomic read density as described above. Normalized read densities for each gene were aligned by the transcription start site and divided into sense and antisense transcripts. The median read density for each gene (from the tss to the end of the coding sequence) was then determined for each transcript. Intron regions were excluded from the calculation.

Author Contributions

RZ optimized ChIP-NChAP and performed all the experiments except the ones in Figure 3 (done by MRL) and Figures S3 and S5 (done by AC). AC assisted RZ in the cell culture and ChIP steps of the experiments. RZ and AC constructed the yeast strains. MRL conceived and developed ChIP-NChAP, designed the experiments with input from RZ and AC, wrote the Perl and R analysis scripts, analyzed the data, and wrote the manuscript.

Acknowledgments

We thank Susan Forsburg, Paul Kaufman, Traci Lee, Etienne Schwob, and Zhiguo Zhang for yeast strains. Thank you to Marta Gut and Julie Blanc from CNAG (Barcelona, Spain) for deep-sequencing services. This work was supported by the ERC-Consolidator (NChIP 647618) grant (MRL).

References

Alabert, C., and Groth, A. (2012). Chromatin replication and epigenome maintenance. Nat Rev Mol Cell Biol *13*, 153-167.

Benson, L.J., Gu, Y., Yakovleva, T., Tong, K., Barrows, C., Strack, C.L., Cook, R.G., Mizzen, C.A., and Annunziato, A.T. (2006). Modifications of H3 and H4 during chromatin replication, nucleosome assembly, and histone exchange. J Biol Chem *281*, 9287-9296.

Bonev, B., and Cavalli, G. (2016). Organization and function of the 3D genome. Nat Rev Genet *17*, 772.

Celic, I., Masumoto, H., Griffith, W.P., Meluh, P., Cotter, R.J., Boeke, J.D., and Verreault, A. (2006). The sirtuins hst3 and Hst4p preserve genome integrity by controlling histone h3 lysine 56 deacetylation. Curr Biol *16*, 1280-1289.

Choe, K.N., and Moldovan, G.L. (2017). Forging Ahead through Darkness: PCNA, Still the Principal Conductor at the Replication Fork. Mol Cell *65*, 380-392.

Coleman, R.T., and Struhl, G. (2017). Causal role for inheritance of H3K27me3 in maintaining the OFF state of a Drosophila HOX gene. Science *356*.

Cusick, M.E., DePamphilis, M.L., and Wassarman, P.M. (1984). Dispersive segregation of nucleosomes during replication of simian virus 40 chromosomes. J Mol Biol *178*, 249-271.
Elliott, S.G. (1983). Coordination of growth with cell division: regulation of synthesis of RNA during the cell cycle of the fission yeast Schizosaccharomyces pombe. Mol Gen Genet *192*, 204-211.
Elliott, S.G., and McLaughlin, C.S. (1978). Rate of macromolecular synthesis through the cell cycle of the yeast Saccharomyces cerevisiae. Proc Natl Acad Sci U S A *75*, 4384-4388.
Foltman, M., Evrin, C., De Piccoli, G., Jones, R.C., Edmondson, R.D., Katou, Y., Nakato, R., Shirahige, K., and Labib, K. (2013). Eukaryotic replisome components cooperate to process histones during chromosome replication. Cell reports *3*, 892-904.
Gan, H., Serra-Cardona, A., Hua, X., Zhou, H., Labib, K., Yu, C., and Zhang, Z. (2018). The Mcm2-Ctf4-Polalpha Axis Facilitates Parental Histone H3-H4 Transfer to Lagging Strands. Mol Cell *72*, 140-151 e143.
Ge, Z., Nair, D., Guan, X., Rastogi, N., Freitas, M.A., and Parthun, M.R. (2013). Sites of acetylation on newly synthesized histone H4 are required for chromatin assembly and DNA damage response signaling. Mol Cell Biol *33*, 3286-3298.
Gerard, A., Koundrioukoff, S., Ramillon, V., Sergere, J.C., Mailand, N., Quivy, J.P., and Almouzni, G. (2006). The replication kinase Cdc7-Dbf4 promotes the interaction of the p150 subunit of chromatin assembly factor 1 with proliferating cell nuclear antigen. EMBO Rep *7*, 817-823.
Gruss, C., Gutierrez, C., Burhans, W.C., DePamphilis, M.L., Koller, T., and Sogo, J.M. (1990). Nucleosome assembly in mammalian cell extracts before and after DNA replication. Embo J *9*, 2911-2922.
Jackson, V., Shires, A., Tanphaichitr, N., and Chalkley, R. (1976). Modifications to histones immediately after synthesis. J Mol Biol *104*, 471-483.
Jiang, C., and Pugh, B.F. (2009). Nucleosome positioning and gene regulation: advances through genomics. Nat Rev Genet *10*, 161-172.
Kaplan, T., Liu, C.L., Erkmann, J.A., Holik, J., Grunstein, M., Kaufman, P.D., Friedman, N., and Rando, O.J. (2008). Cell cycle- and chaperone-mediated regulation of H3K56ac incorporation in yeast. PLoS Genet *4*, e1000270.
Kaufman, P.D., Kobayashi, R., Kessler, N., and Stillman, B. (1995). The p150 and p60 subunits of chromatin assembly factor I: a molecular link between newly synthesized histones and DNA replication. Cell *81*, 1105-1114.
Kim, T.S., Liu, C.L., Yassour, M., Holik, J., Friedman, N., Buratowski, S., and Rando, O.J. (2010). RNA polymerase mapping during stress responses reveals widespread nonproductive transcription in yeast. Genome Biol *11*, R75.
Kornberg, R.D., and Lorch, Y. (1999). Twenty-five years of the nucleosome, fundamental particle of the eukaryote chromosome. Cell *98*, 285-294.
Laprell, F., Finkl, K., and Muller, J. (2017). Propagation of Polycomb-repressed chromatin requires sequence-specific recruitment to DNA. Science *356*, 85-88.
Li, Q., Zhou, H., Wurtele, H., Davies, B., Horazdovsky, B., Verreault, A., and Zhang, Z. (2008). Acetylation of histone H3 lysine 56 regulates replication-coupled nucleosome assembly. Cell *134*, 244-255.
Liu, C.L., Kaplan, T., Kim, M., Buratowski, S., Schreiber, S.L., Friedman, N., and Rando, O.J. (2005). Single-nucleosome mapping of histone modifications in S. cerevisiae. PLoS Biol *3*, e328.
Liu, C.L., Schreiber, S.L., and Bernstein, B.E. (2003). Development and validation of a T7 based linear amplification for genomic DNA. BMC Genomics *4*, 19.
Luger, K., Mader, A.W., Richmond, R.K., Sargent, D.F., and Richmond, T.J. (1997). Crystal structure of the nucleosome core particle at 2.8 A resolution. Nature *389*, 251-260.
Masumoto, H., Hawke, D., Kobayashi, R., and Verreault, A. (2005). A role for cell-cycle-regulated histone H3 lysine 56 acetylation in the DNA damage response. Nature *436*, 294-298.
Mattiroli, F., Gu, Y., Yadav, T., Balsbaugh, J.L., Harris, M.R., Findlay, E.S., Liu, Y., Radebaugh, C.A., Stargell, L.A., Ahn, N.G.*, et al.* (2017). DNA-mediated association of two histone-bound complexes of

yeast Chromatin Assembly Factor-1 (CAF-1) drives tetrasome assembly in the wake of DNA replication. Elife *6*.
Millar, C.B., and Grunstein, M. (2006). Genome-wide patterns of histone modifications in yeast. Nat Rev Mol Cell Biol *7*, 657-666.
Nieduszynski, C.A., Hiraga, S., Ak, P., Benham, C.J., and Donaldson, A.D. (2007). OriDB: a DNA replication origin database. Nucleic Acids Res *35*, D40-46.
Petryk, N., Dalby, M., Wenger, A., Stromme, C.B., Strandsby, A., Andersson, R., and Groth, A. (2018). MCM2 promotes symmetric inheritance of modified histones during DNA replication. Science.
Radman-Livaja, M., and Rando, O.J. (2010). Nucleosome positioning: how is it established, and why does it matter? Dev Biol *339*, 258-266.
Rando, O.J. (2007). Global patterns of histone modifications. Curr Opin Genet Dev *17*, 94-99.
Rando, O.J., and Ahmad, K. (2007). Rules and regulation in the primary structure of chromatin. Curr Opin Cell Biol *19*, 250-256.
Razin, S.V., Iarovaia, O.V., Sjakste, N., Sjakste, T., Bagdoniene, L., Rynditch, A.V., Eivazova, E.R., Lipinski, M., and Vassetzky, Y.S. (2007). Chromatin domains and regulation of transcription. J Mol Biol *369*, 597-607.
Rege, M., Subramanian, V., Zhu, C., Hsieh, T.H., Weiner, A., Friedman, N., Clauder-Munster, S., Steinmetz, L.M., Rando, O.J., Boyer, L.A*., et al.* (2015). Chromatin Dynamics and the RNA Exosome Function in Concert to Regulate Transcriptional Homeostasis. Cell Reports *13*, 1610-1622.
Rohland, N., and Reich, D. (2012). Cost-effective, high-throughput DNA sequencing libraries for multiplexed target capture. Genome Res *22*, 939-946.
Sauer, P.V., Timm, J., Liu, D., Sitbon, D., Boeri-Erba, E., Velours, C., Mucke, N., Langowski, J., Ochsenbein, F., Almouzni, G*., et al.* (2017). Insights into the molecular architecture and histone H3-H4 deposition mechanism of yeast Chromatin assembly factor 1. Elife *6*.
Sobel, R.E., Cook, R.G., Perry, C.A., Annunziato, A.T., and Allis, C.D. (1995). Conservation of deposition-related acetylation sites in newly synthesized histones H3 and H4. Proc Natl Acad Sci U S A *92*, 1237-1241.
Talarek, N., Petit, J., Gueydon, E., and Schwob, E. (2015). EdU Incorporation for FACS and Microscopy Analysis of DNA Replication in Budding Yeast. Methods Mol Biol *1300*, 105-112.
Tran, V., Lim, C., Xie, J., and Chen, X. (2012). Asymmetric division of Drosophila male germline stem cell shows asymmetric histone distribution. Science *338*, 679-682.
Vasseur, P., Tonazzini, S., Ziane, R., Camasses, A., Rando, O.J., and Radman-Livaja, M. (2016). Dynamics of Nucleosome Positioning Maturation following Genomic Replication. Cell Reports *16*, 2651-2665.
Voichek, Y., Bar-Ziv, R., and Barkai, N. (2016). Expression homeostasis during DNA replication. Science *351*, 1087-1090.
Voichek, Y., Mittelman, K., Gordon, Y., Bar-Ziv, R., Lifshitz Smit, D., Shenhav, R., and Barkai, N. (2018). Epigenetic Control of Expression Homeostasis during Replication Is Stabilized by the Replication Checkpoint. Mol Cell *70*, 1121-1133 e1129.
Wang, X., and Moazed, D. (2017). DNA sequence-dependent epigenetic inheritance of gene silencing and histone H3K9 methylation. Science *356*, 88-91.
Xie, J., Wooten, M., Tran, V., Chen, B.C., Pozmanter, C., Simbolon, C., Betzig, E., and Chen, X. (2015). Histone H3 Threonine Phosphorylation Regulates Asymmetric Histone Inheritance in the Drosophila Male Germline. Cell *163*, 920-933.
Xu, Z., Wei, W., Gagneur, J., Perocchi, F., Clauder-Munster, S., Camblong, J., Guffanti, E., Stutz, F., Huber, W., and Steinmetz, L.M. (2009). Bidirectional promoters generate pervasive transcription in yeast. Nature *457*, 1033-1037.
Yang, J., Zhang, X., Feng, J., Leng, H., Li, S., Xiao, J., Liu, S., Xu, Z., Xu, J., Li, D*., et al.* (2016). The Histone Chaperone FACT Contributes to DNA Replication-Coupled Nucleosome Assembly. Cell Reports *16*, 3414.

Yang, S.C., Rhind, N., and Bechhoefer, J. (2010). Modeling genome-wide replication kinetics reveals a mechanism for regulation of replication timing. Mol Syst Biol *6*, 404.
Yu, C., Gan, H., Han, J., Zhou, Z.X., Jia, S., Chabes, A., Farrugia, G., Ordog, T., and Zhang, Z. (2014). Strand-specific analysis shows protein binding at replication forks and PCNA unloading from lagging strands when forks stall. Mol Cell *56*, 551-563.
Yu, C., Gan, H., Serra-Cardona, A., Zhang, L., Gan, S., Sharma, S., Johansson, E., Chabes, A., Xu, R.M., and Zhang, Z. (2018). A mechanism for preventing asymmetric histone segregation onto replicating DNA strands. Science.

Figure Legends

Figure 1: Early S-phase RNAPol2 ChIP-NChAP results. A. Correlation between the 255 gene moving window average of the median RNAPol2 occupancy (RNAPol2 ChIP/input) in the coding sequence of each yeast gene (excluding promoters) and gene replication timing (Vasseur et al., 2016). RNA pol2 occupancy was measured in synchronized wt cells in early (25min after release from G1 arrest) and mid-early (32min) S-phase by HA tagged RNAPol2 ChIP hybridized to whole genome two channel microarrays (4x44K Agilent), occupancy values are an average of two dye flip technical replicates (Top). Bottom: Difference in average log2(RNAPol2/input) between early and late genes (blue) and mid early and late genes (red) in asynchronous cultures, and in early and mid-early S-phase. As replication in the cell population progresses RNAPol2 occupancy relative to gene copy number decreases, i.e. earlier replicated genes have less RNAPol2 per gene copy than late genes that have not yet been replicated; compare early replicating genes (replication timing <43min) or mid early replicating genes (43min<=replication timing<55min) to late replicating genes (replication timing >=55min) in red (early S) and green (mid early S) curves in the top panel, and in the bar graph in the bottom panel. Conversely RNAPol2 occupancy in asynchronous cells (blue, (Kim et al., 2010)) shows the expected pattern of higher occupancy in early genes compared to late genes as early genes are known to have on average higher transcriptional activity than late replicating genes. Ratio values on the Y axis have been normalized to 0 by subtracting the average log2(RNAPol2/input) for all genes from the log2(RNAPol2/input) for each gene. Release media contained 10uM EdU**. B.** Diagram of the RNAPol2 ChIP-NChAP experiment. **C.** RNAPol2 distribution on chromosome 9 from chromatin fractions diagramed on the left 25min (early S-phase) after release from G1arrest (blue bars). The positions of replication origins (ARS) are shown in the three bottom rows: 1. previously documented ARS; 2.ARS identified in Vasseur et al, 2016, and 3. ARS from this study. Notice that NChAP from early S-phase (this dataset) reveals clusters of replication origins at loci where only single origins were identified later in S-phase(two previous rows). Read counts were grouped in 50 bp bins and first normalized to the genome average read count and then to the highest peak value in each chromosome. RADs are

replication associated domains i.e. regions that have been replicated 25min after release as determined in Vasseur et al. (2016). W and C are Watson and Crick strand reads , respectively.

Figure 2: Asymmetric distribution of RNAPol2 on replicated gene copies. A. Heat map of median RNAPol2 occupancies in coding regions (CDS) of all yeast genes. Each line is an individual gene and columns represent occupancy values for (W)atson and (C)rick gene copies for different G1 and S-phase time points (late G1 (after 3.75 hrs in alpha factor, 100% of the genome is non-replicated, 2 replicates), early S (54% of the genome is non-replicated over the whole cell population), early-mid S (21% non-replicated), mid early S (replicate 1, 10% non-replicated), and mid early S (replicate 2, 10% non-replicated), from the ChIP, NChAP (nascent chromatin) and ChIP-NChAP (Nascent RNAPol2) fractions. The first two columns on the left represent mRNA enrichment over G1 genomic DNA in mid and late S (in the absence of EdU) determined with gene expression microarrays (Vasseur et al., 2016). The scatter plot on the right shows the correlation between bulK RNAPol2 occupancies in early-mid and mid-early S (repl. 1) and mRNA abundance in mid S. Genes are grouped by cell cycle expression patterns and then ordered by replication timing within each group (replication timing determined in Vasseur et al., 2016). Median read density values for each gene have been normalized by separately dividing the W and C read densities of each gene in the ChIP and NChAP fractions with the W and C average read density of the sonicated input fraction for the same gene. The ChIP-NChAP medians have been normalized by dividing the W and C values with the input normalized W and C average values from the ChIP fraction. The non-replicated ChIP fractions from early (54% non-replicated) and mid early S (10% non-replicated, repl. 2) show RNAPol2 enrichment (yellow/red) in non-replicated genes (blue genes in the NChAP fractions) relative to replicated ones (blue/yellow), in contrast to bulk ChIP fractions from early-mid S (21% non-replicated), mid early S (replicate 1, 10% non-replicated). This indicates that we are succesfully separating RNAPol2 bound nascent chromatin from RNAPol2 bound non-replicated chromatin. **B**. W versus C copies scatter plot of median normalized (as in A) read densities of early replicating genes(shown in A) for RNAPol2 on nascent chromatin (ChIP-NChAP fraction, blue), nascent chromatin (NChAP fraction, red), and RNAPol2 on non-replicated chromatin (ChIP non-replicated fraction, green). The biggest differences between the two replicated copies are seen in the ChIP-NChAP fraction, suggesting asymmetrical distribution of RNAPol2. **C** Scatter plot of the ratio of RNAPol2 occupancy between the lagging and the leading gene copy for all 705 early genes from B and the average median RNAPol2 density (average of W and C copies) on nascent chromatin (blue) and non-replicated chromatin (green). **D**. Early genes (705 genes from B and C) were sorted by

increasing lagging/leading nascent RNAPol2 ratio and then divided into 7 bins of ~100 genes each, and we determined the box plot distribution of lagging/leading ratios for each bin (right panel), average lagging/leading ratios for each bin are in the y axis. For example the bottom group of genes has on average 5.6 times more RNAPol2 on the leading copy than on the lagging. We then calculated the ratio of "same" orientation genes versus "opposite" genes for each group normalized to the same/opposite ratio of all 705 genes (bar graph, left panel). As predicted, "same" gene enrichment is inversely proportional to the nascent RNAPol2 lagging/leading ratio, i.e. "same" genes in early S-phase tend to have more RNA pol2 on the leading copy and "opposite" genes tend to have more RNAPol2 on the lagging copy. **E**. Box plot distributions of lagging/leading nascent RNA pol2 ratios from early to mid-early S-phase (columns left to right) for early (second and third rows from the top) and mid-early genes (two bottom rows) (r.t. = replication timing). The top row shows the distribution of genome read densities (in 400bp bins) normalized to the maximum read density for each NChAP fraction (reads have not been normalized to input) at indicated time points in S-phase. In early S-phase 54% of the genome has a read density of 0, i.e. 54% of the genome has not yet been replicated, and ~5% of the genome has a read density of 4, i.e. 4% of the population has replicated 5% of their genome. By mid-early S-phase 50% of cells have replicated at least 0.5% of their genomes and only 10% of the genome has not been replicated in the whole cell population. In the second and fourth rows from the top genes have been sorted by increasing lagging/leading RNAPol2 occupancy in early S-phase and divided into 7 bins as in C (y axis), and box plot distribution of nascent RNAPol2 lagging/leading ratios (x axis) have been determined for each bin at indicated time points. Rows 3 and 5: same as 2 and 3 except that genes have been ordered by increasing lagging/leading RNAPol2 ratios from mid-early S (replicate 1). The bar graphs on the left show the "same" gene enrichment calculated as in C for gene bins indicated in the Y axis of each row on the right.

Figure 3: Asymmetric distribution of new histones on daughter chromatids in S-phase. A. H3K56ac distribution on chromosome 9 from chromatin fractions diagramed on the left: midlog, G1 arrest, 24min(early S-phase) and 30min(mid S-phase) after release (each gene is represented with a different color). The positions of replication origins (ARS) are shown in the three bottom rows as in Figure 1C. Read counts were grouped in 400 bp bins and first normalized to the average genome read count and then to the highest peak value in each chromosome. W and C are Watson and Crick strand reads, respectively. **B.** Box plot distributions of lagging/leading nascent H3K56ac (dark blue) and nascent RNAPol2 (light blue) ratios from early (left) and mid (right) S-phase for early (third and fifth rows) and mid-early genes (fourth and sixth rows). The top two rows show the distribution of genome

read densities (in 400bp bins) normalized to the maximum read density for each dataset: left: nascent chromatin early Sphase replicate 1 from Figure 2D (54% non-replicated) (top); nascent chromatin from early S-phase (MNase-NChAP from A, 60% non-replicated) (bottom); right: nascent chromatin mid-early Sphase replicate 1 from Figure 2D (10% non-replicated) (top); bulk H3K56ac ChIP from mid S-phase (H3K56ac ChIP mid-S-phase from A, 6% non-replicated) (bottom), reads have not been normalized to input. Since H3K56ac is a mark of new histones, H3K56ac ChIP in mid S-phase can serve as a proxy for measuring the fraction of the genome replicated in the cell population as with NChAP fractions. By mid S-phase 15% of cells have replicated at least 3% of their genomes and only 6% of the genome has not been replicated in the whole cell population. Rows 3 and 4: early and mid-early genes have been sorted by increasing lagging/leading RNAPol2 occupancy from early S-phase (replicate 1, Figure 2), respectively, and then divided into 7 bins as in Figure 2C-D (y axis), and box plot distributions of nascent H3K56ac lagging/leading ratios (x axis) from early (left) and mid (right) S-phase have been determined. The bar graphs on the left show the "same" gene enrichment calculated as in Figure 2C-D for gene bins indicated in the Y axis of each row on the right. Rows 5 and 6: as rows 3 and 4 but sorted by increasing lagging/leading RNAPol2 occupancy from mid-early S-phase (replicate 1, Figure 2), respectively.

Figure 4: Asymmetric distribution of RNAPol2 on replicated gene copies in rtt109D cells. A.Heat map of median RNAPol2 occupancies in coding regions (CDS) of all yeast genes. Each line is an individual gene and columns represent occupancy values for (W)atson and (C)rick gene copies for early-mid S-phase after release from G1 arrest in rtt109D(10% non-replicated,3 biological replicates) and wt (10% non-replicated replicate 1 from Figure 2) cells, from the ChIP, NChAP (nascent chromatin) and ChIP-NChAP (Nascent RNAPol2) fractions. The first two columns on the left represent mRNA enrichment over G1 genomic DNA in mid S (in the absence of EdU) determined with gene expression microarrays (Vasseur et al., 2016) in rtt109D (average of 3 replicates) and wt (average of 2 replicates) cells(Figure S2). Genes are grouped by cell cycle expression patterns and then ordered by replication timing within each group (replication timing determined in Vasseur et al., 2016). Median read density values for each gene have been normalized by separately dividing the W and C read densities of each gene in the bulk ChIP and NChAP fractions with the W and C average read density of the sonicated input fraction for the same gene. The ChIP-NChAP medians have been normalized by separately dividing the W and C values with the input normalized W and C average values from the ChIP fraction. **B.** 100 gene moving window average of median RNAPol2 enrichment (RNAPol2 ChIP/input) from indicated bulk ChIP datasets versus mRNA enrichment over G1 DNA in wt (left) and rtt109D (right). The

range of relative RNAPol2 enrichment/depletion is significantly diminished in rtt109D replicates 1 and 2 compared to wt. In rtt109D replicate 3 on the other hand, the mean RNAPol2 occupancy is reduced relative to wt. This suggests that RNAPol2 occupancy is globally reduced in rtt109D mutants in agreement with spike-in normalized RNA-seq results shown in Fig S3. **C**. Average RNAPol2 density at early, mid-early and late replicating genes (replication timing as measured in Vasseur et al., 2016) for the three rtt109D replicates and the wt replicate from A and B . Buffering of RNAPol2 occupancy appears to be lost in rtt109D cells. Unlike in wt cells, in rtt109D cells RNAPol2 occupancy relative to gene copy number is not reduced at replicated genes compared to unereplicated genes (compare early (blue) and mid-early (red) genes to late genes (green). Enrichment ratios on the Y axis have been normalized to 0 by subtracting the average log2(RNAPol2/input) for all genes from the log2(RNAPol2/input) for each gene. **D**. Box plot distributions of lagging/leading nascent RNA pol2 ratios from early (wt) to mid-early S-phase (wt and rtt109D, columns left to right) for early (second to fourth rows from the top) and mid-early genes (three bottom rows) (r.t.= replication timing). Top row: distribution of genome read densities (in 400bp bins) normalized to the maximum read density for each NChAP fraction (reads have not been normalized to input) at indicated time points in S-phase as in Fig.2. Rows 2 and 4 from the top: genes have been sorted by increasing lagging/leading RNAPol2 occupancy in early S-phase (wt, Fig. 2) and divided into 7 bins as in Fig.2 C-D (y axis), and box plot distributions of nascent RNAPol2 lagging/leading ratios (x axis) have been determined for each bin at indicated time points. Rows 3,6 and 4,7: same as 2 and 4 except that genes have been ordered by increasing lagging/leading RNAPol2 ratios from rtt109D (replicate 1) or mid-early S (replicate 1, wt Fig. 2), respectively. The bar graphs on the left show “same” gene enrichments calculated as in Fig2 C-D for gene bins indicated in the Y axis of each row on the right. The RNAPol2 distribution pattern between leading and lagging strand gene copies in rtt109D cells correlates with wt, indicating that the asymmetric distribution of RNAPol2 on replicated DNA does not depend on H3K56Ac, and the observed rtt109D “effect” on transcription buffering is more likely due to the global decrease in RNAPol2 occupancy.

Figure 5: EdU pulse chase in an asynchronous culture. H3K56ac and Rpb3 distribution on nascent chromatin. A. Experimental outline. **B.** Scatter plot simulations based on predictions for two RNAPol2 distribution models. The plots show the expected nascent RNAPol2 enrichments on the lagging strand (Log2 (lagging/leading)) 7 or 15 min after EdU addition versus the ratio of lagging/leading RNAPol2 enrichments between 15min and 7min after EdU addition. Each plot has 1200 data points generated by the Excel Random Number Generation function with a normal distribution. Left: prediction for a two-step model of H3K56ac binding to nascent DNA with initial enrichment on the leading strand

followed by a switch to the lagging strand. Right: Alternating two step model with RNAPol2 enriched on the leading strand at 7min and on the lagging at 15min for "same" genes and vice-versa for "opposite" genes. **C.** Heat map of median RNAPol2 (Rpb3) and H3K56ac enrichments over input in bulk and nascent chromatin for CDSes of 431 genes replicated from efficient origins identified in Vasseur et al. 2016. Genes are ordered by increasing change in lagging/leading (lg/ld) ratios of nascent Rpb3 enrichment between 15 and 7 min time points from replicate 2. The last column on the right shows the genic orientation of each gene (same- red and opposite-blue). H3K56ac and Rpb3 ChIPs and ChIP-NChAPs were done in parallel for each replicate. The smaller heat map on the right shows the Pearson correlation between lg/ld enrichment ratios for H3K56ac and Rpb3 from each time point and each replicate. H3K56ac distribution patterns correlate well between replicates for the 15min timepoints and less well for the 7min time points, while H3K56ac distribution has no correlation with RNAPol2 distribution even within the same replicate. **D.-E.** Top: Scatter plots as in B with experimental data from C: Rpb3 (D) and H3K56ac (E) from replicates 1 and 2. The plots resemble the prediction for model 2 (B. right). Bottom: Genic orientation (same: 1 and opposite:-1) for each gene from C. versus nascent Rpb3 log2(15min(lg/ld)/7min(lg/ld)) (D) or nascent H3K56Ac log2(15min(lg/ld)/7min(lg/ld)) (E). Rpb3 enrichment switches from leading to lagging copies for predominantly "same" genes and from lagging to leading for predominantly "opposite" genes as predicted in B (right panel). At the same time, H3K56ac enrichment switches in the opposite direction: from lagging to leading for mostly "opposite" genes and from lagging to leading for mostly "same". **F.-G**. Average tss centered gene profiles for RNAPol2 (F) and H3K56Ac (G) from nascent (top) and bulk (bottom) chromatin from replicate 2. Genes from C were divided into four groups of equal size (~107 genes in each group) according to the magnitude of the change in the median read density lagging/leading ratio from the 7min to the 15min time point for RNAPol2 (F) and H3K56Ac (G) (blue strip on the left of the plots) as described in C-E. The average input normalized read densities 500bp upstream and 3kbp downstream of the tss were determined for each gene group for the lagging (blue) and leading (red) gene copies at the 7min (solid line) and 15min (dashed line) time points. Bulk chromatin profiles show no differences between lagging and leading copies. As expected gene bodies from the nascent chromatin fraction are enriched for H3K56ac relative to gene bodies in the bulk chromatin fraction (top and bottom panels in G). The diagram in the middle illustrates the proposed steps for RNAPol2 and H3K56ac distribution on the leading and lagging gene copies after the passage of the fork for "same" (mostly in the bottom two groups) and "opposite" genes (mostly in the top two groups). Nucleosomes (old (red circles) and new (tan circles)) were drawn within genes only, for clarity sake. RNAPol2 is represented as a green arrow and the replication fork as a red triangle.

Figure 6: A. An alternating two-step model for chromatin assembly on daughter chromatids. Nucleosome deposition follows a two-step process, with "old" nucleosomes (red) and RNAPol2 (green arrow) binding first to the leading strand behind the fork while the lagging strand is still maturing. New nucleosomes (tan) will be incorporated into the leading strand mostly at promoters and ends of genes through replication independent turnover. When Okazaki fragments are ligated new nucleosomes acetylated on H3K56, H4K5 and H4K12 are deposited on the lagging strand. RNAPol2 also then apparently "switches" from the leading to the lagging gene copy. Amongst early replicating genes in early S-phase, same orientation genes are mostly still on step 1 and "opposite" genes are already on step 2 of chromatin assembly. By the time the fork is at a distance d1 from the promoter and Okazaki fragments upstream of that point have matured, "opposite" genes have been entirely replicated and both copies have been chromatinized while at "same" genes the coding region of the lagging copy has not yet matured. In mid-early S-phase, the pattern is reversed for mid-early replicating genes: same genes are on step 2 and opposite genes are still on step 1. This is a consequence of progressive slowing down of forks as they advance through opposite genes (which tend to cluster together), which delays the timing of replication of "opposite" genes compared to "same" genes. Deacetylation of H3K56ac in the gene body of the lagging copy causes an apparent shift in H3K56ac enrichment to the leading copy followed by another switch of RNAPol2 to the leading copy in step 3. **B.** Transcription buffering during the cell cycle. The leading strand copy containing old nucleosomes (red) is transcribed first immediately after replication. Later on after Okazaki fragments have been ligated and new acetylated nucleosomes (yellow) have been assembled on the lagging strand copy, transcription shifts to that gene copy. The lagging strand copy is preferentially transcribed through G2 until histone deacetylases acetylation mark at the G2/M transition. After deacetylation nucleosomes from the two daughter copies are indistinguishable (colored red on both copies) and mother and daughter cells inherit identical chromatin configurations. **C.** Modulation of fork velocity or Okazaki maturation rates determines the pattern of old and new nucleosome segregation.

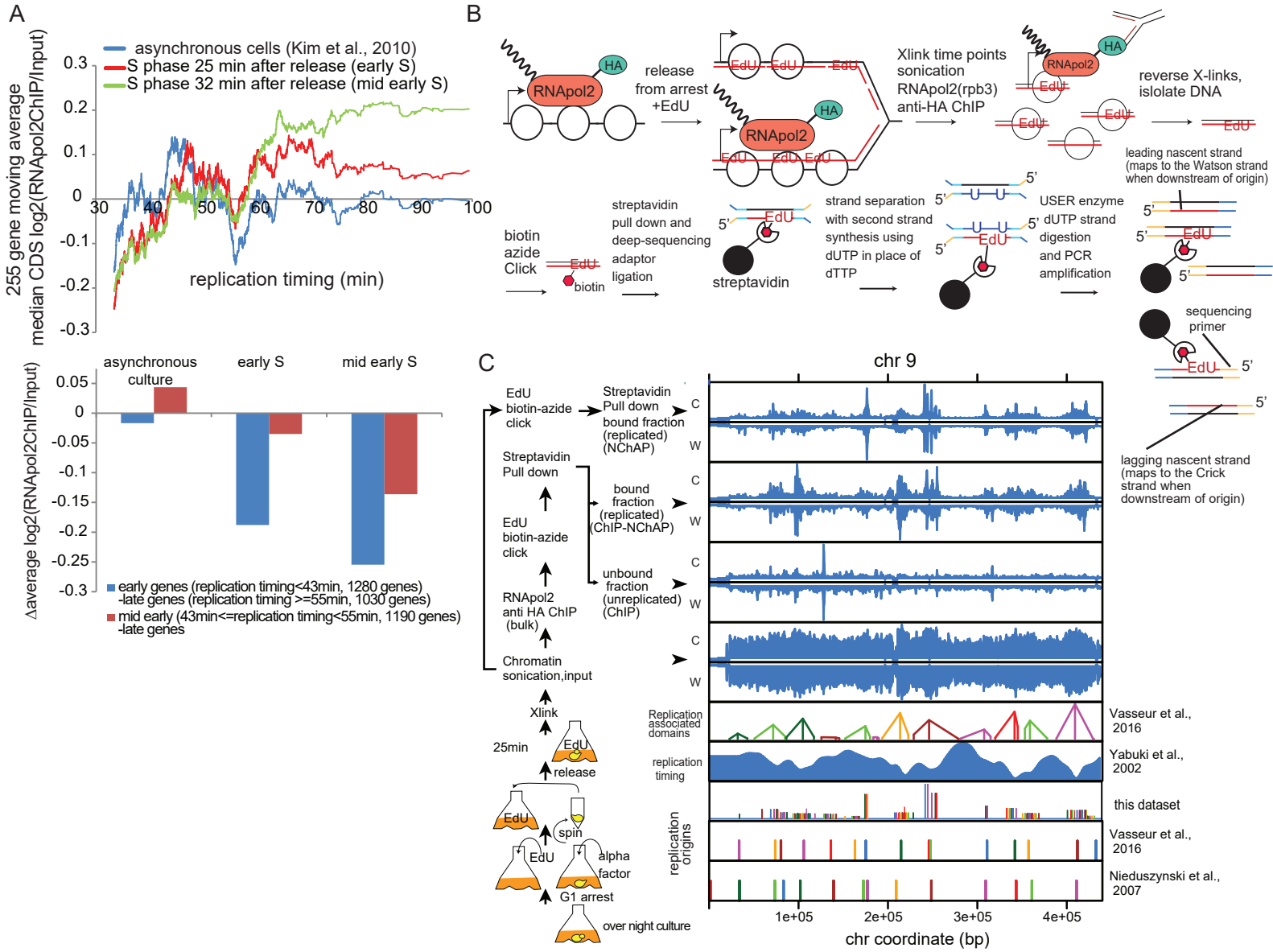
A
asynchronous cells (Kim et al., 2010)
S phase 25 min after release (early S)
S phase 32 min after release (mid early S)
255 gene moving average median CDS log2(RNApol2ChIP/Input)
replication timing (min)
asynchronous culture
early S
mid early S
Δaverage log2(RNApol2ChIP/Input)
early genes (replication timing<43min, 1280 genes) -late genes (replication timing >=55min, 1030 genes)
mid early (43min<=replication timing<55min, 1190 genes) -late genes
B
RNApol2
HA
release from arrest +EdU
Xlink time points sonication RNApol2(rpb3) anti-HA ChIP
reverse X-links, islolate DNA
biotin azide Click
biotin
streptavidin pull down and deep-sequencing adaptor ligation
streptavidin
strand separation with second strand synthesis using dUTP in place of dTTP
USER enzyme dUTP strand digestion and PCR amplification
leading nascent strand (maps to the Watson strand when downstream of origin)
sequencing primer
lagging nascent strand (maps to the Crick strand when downstream of origin)
C
chr 9
EdU biotin-azide click
Streptavidin Pull down bound fraction (replicated) (NChAP)
Streptavidin Pull down
bound fraction (replicated) (ChIP-NChAP)
EdU biotin-azide click
unbound fraction (unreplicated) (ChIP)
RNApol2 anti HA ChIP (bulk)
Chromatin sonication,input
Xlink
25min
release
spin
alpha factor
G1 arrest
over night culture
Replication associated domains
replication timing
replication origins
Vasseur et al., 2016
Yabuki et al., 2002
this dataset
Vasseur et al., 2016
Nieduszynski et al., 2007
chr coordinate (bp)

Figure 1

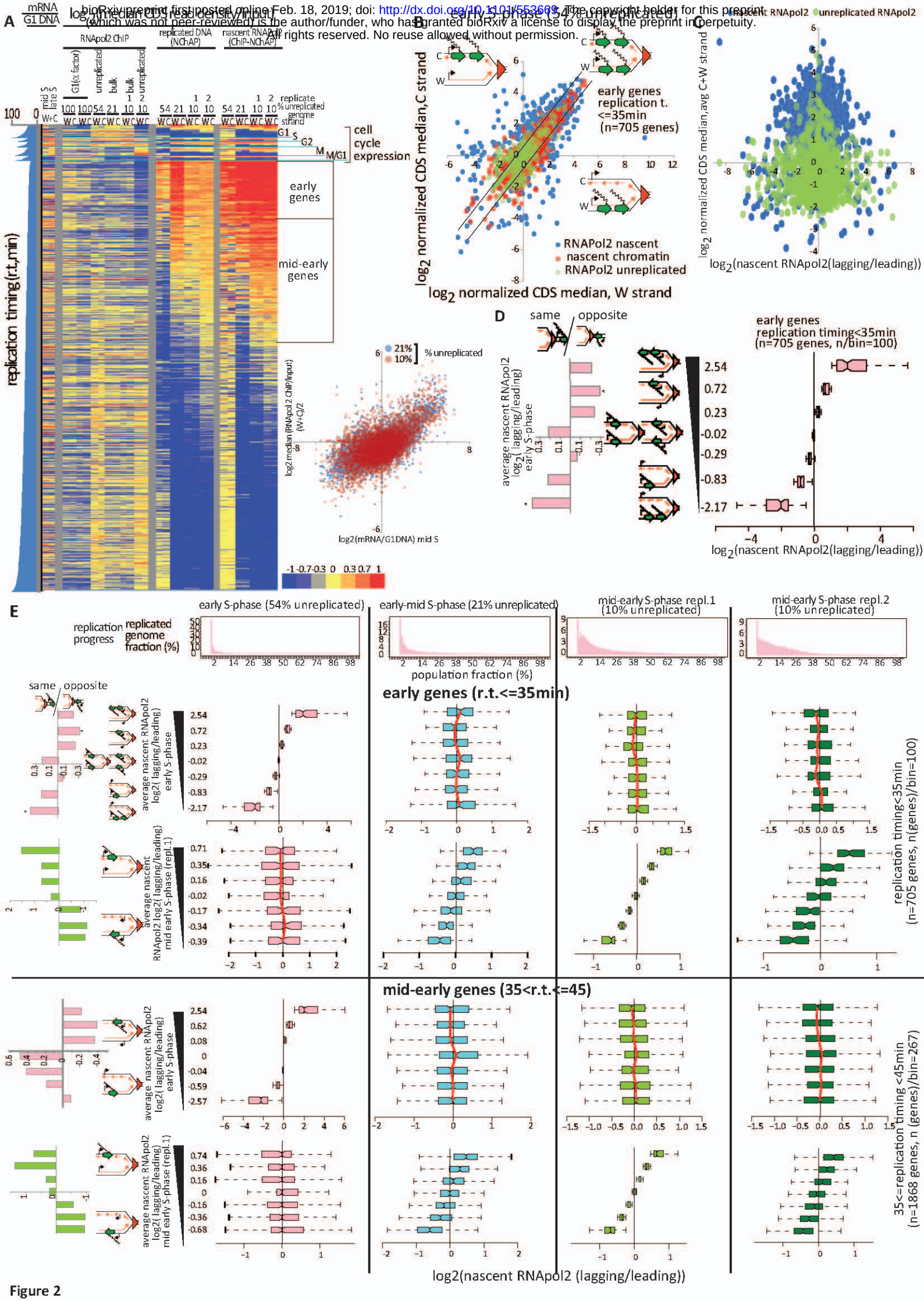

Figure 2

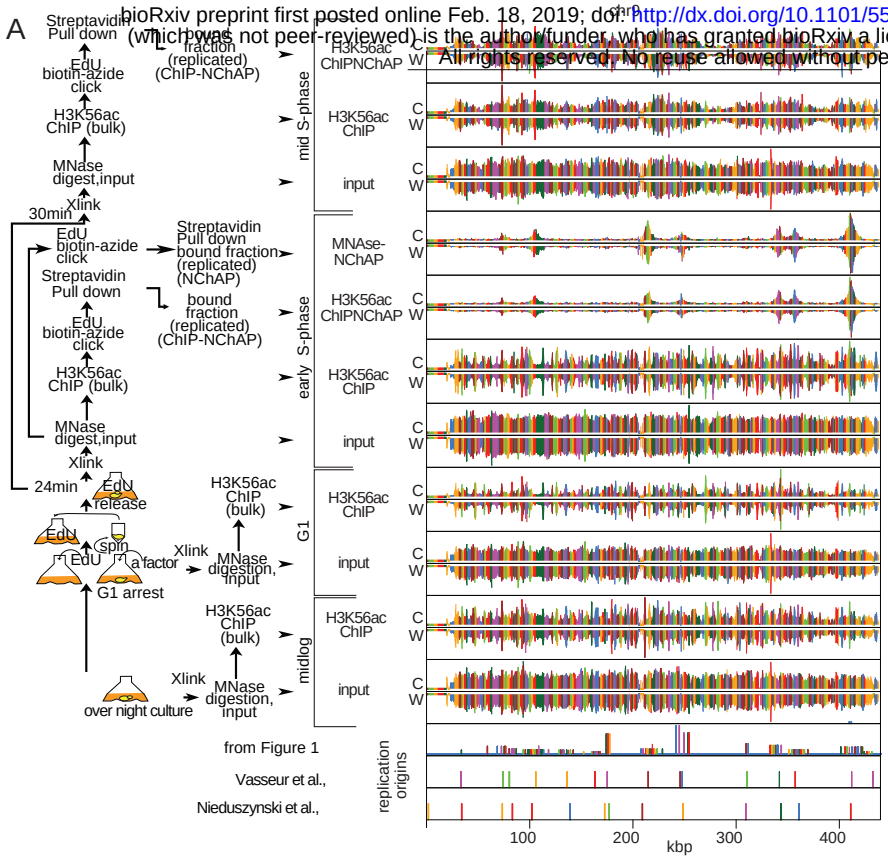

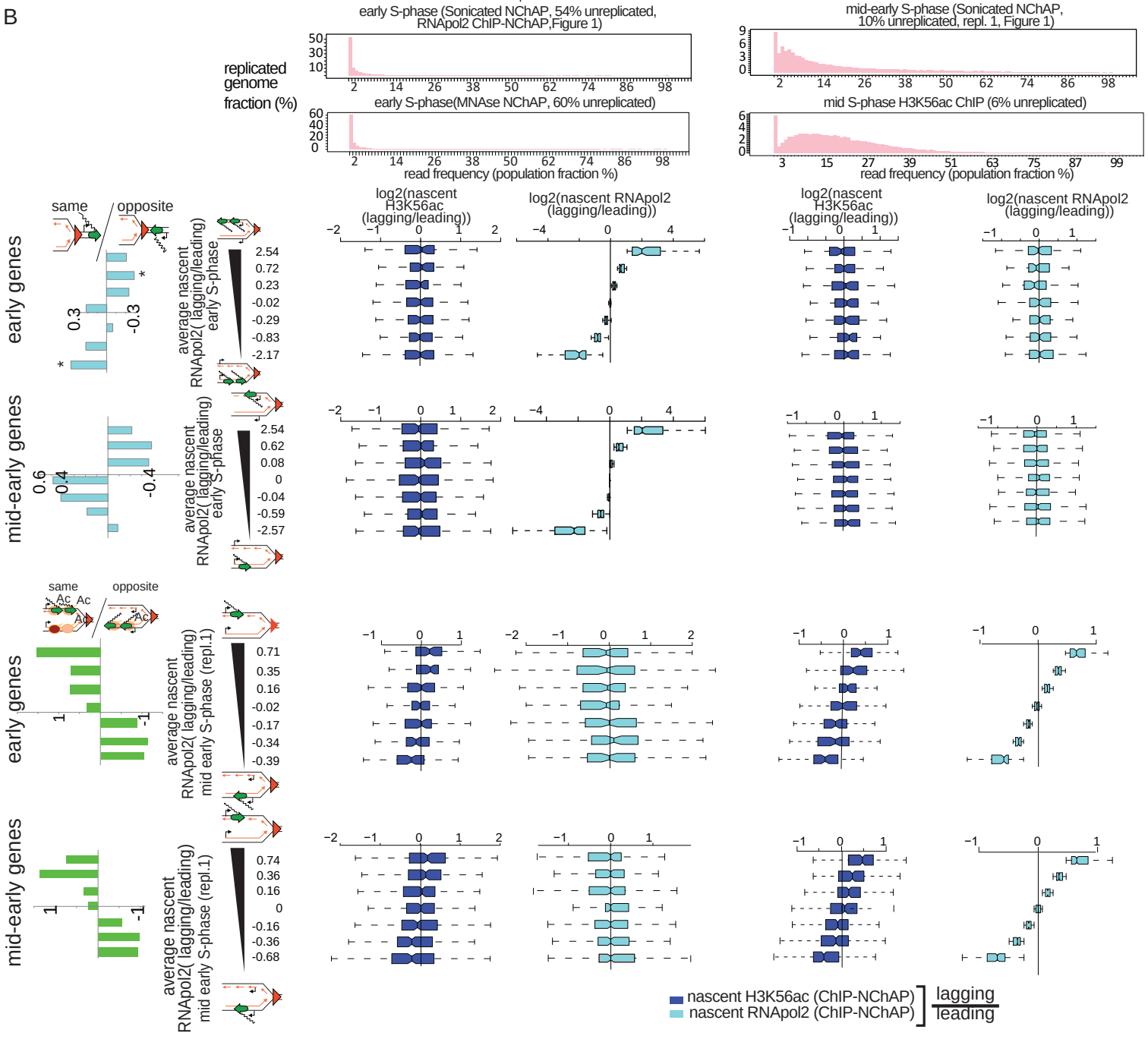

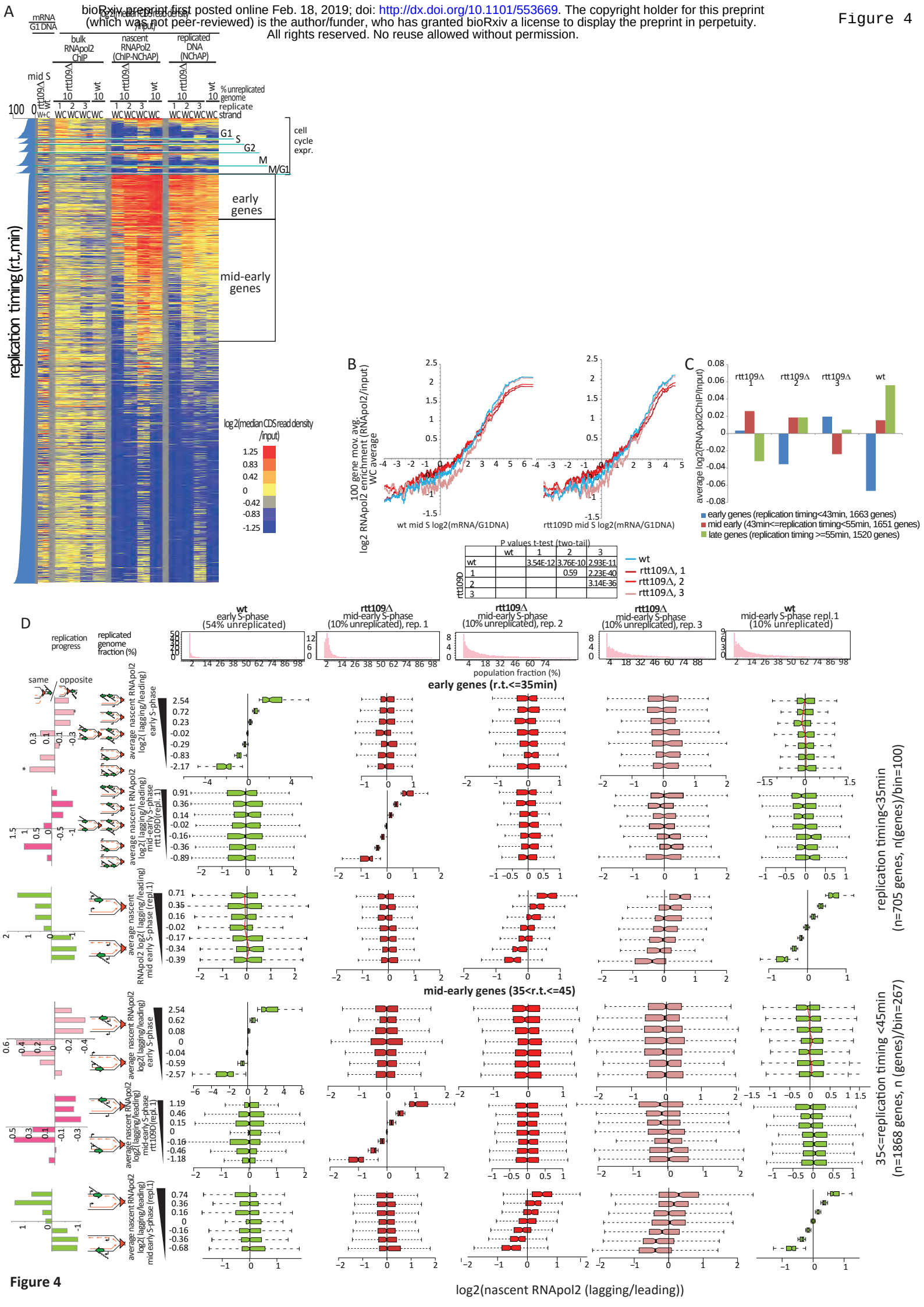

Figure 4

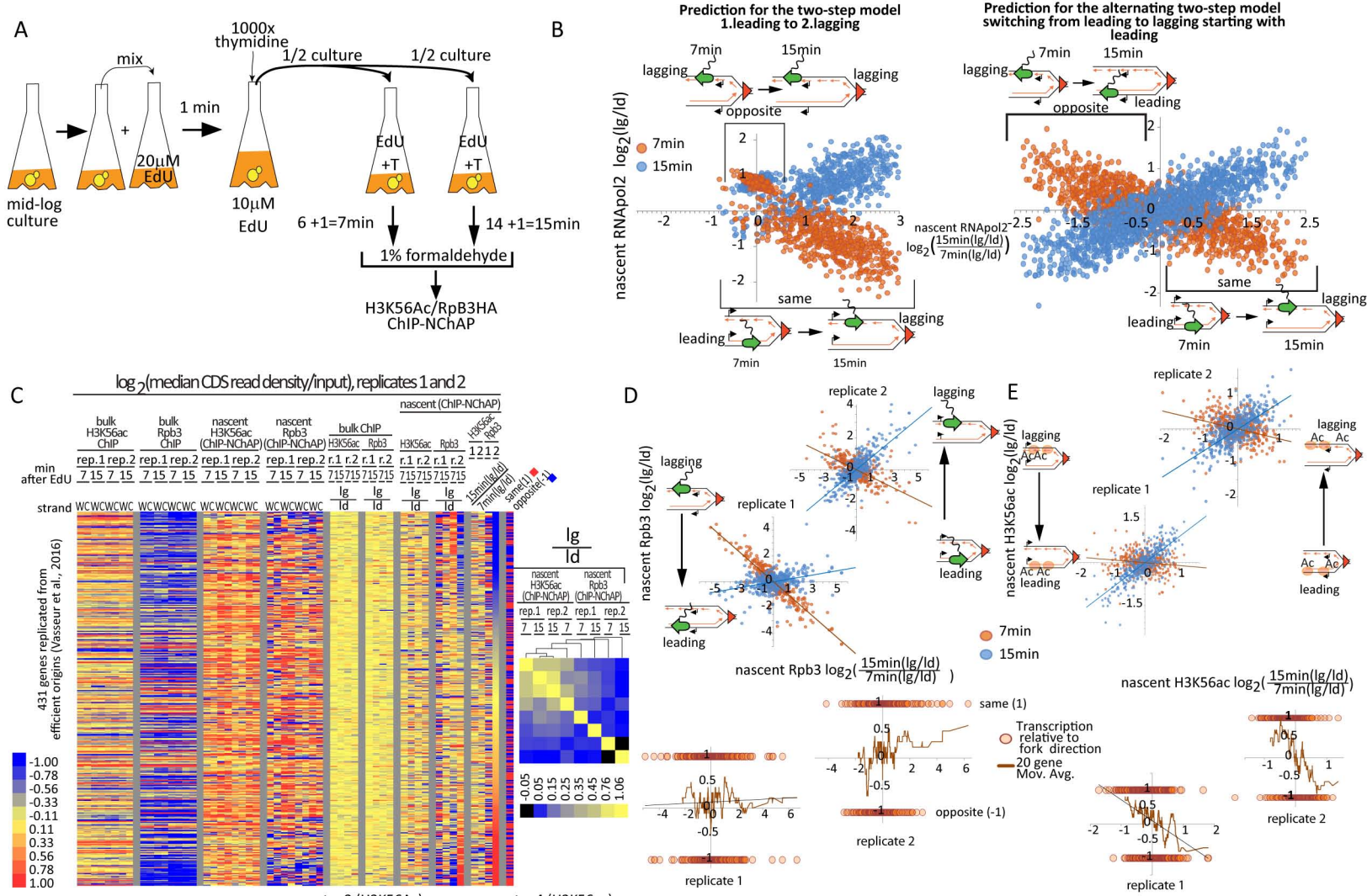

Figure 5

Figure 5

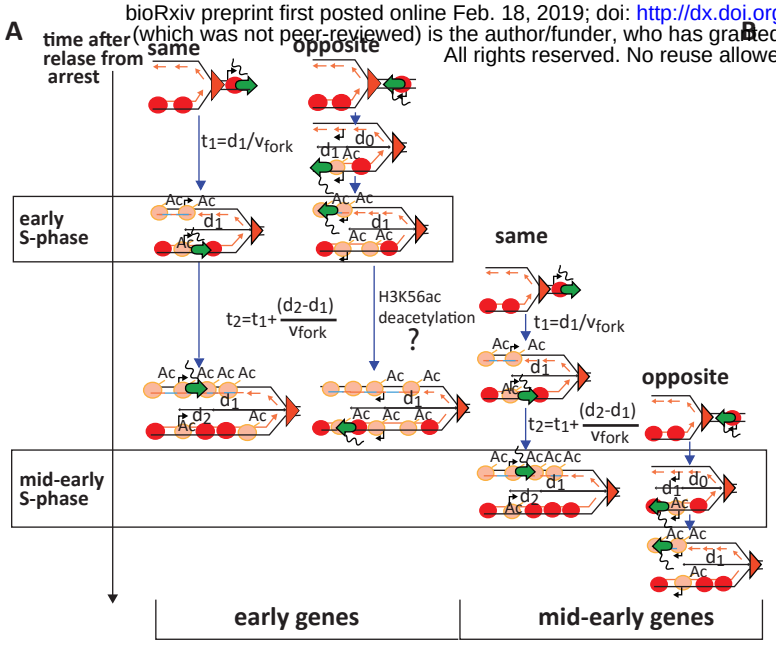

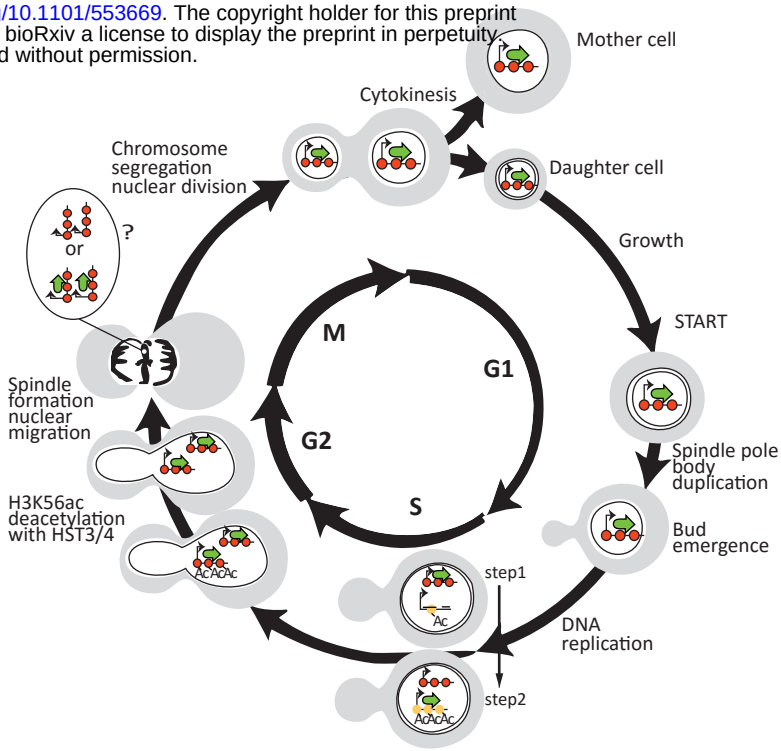

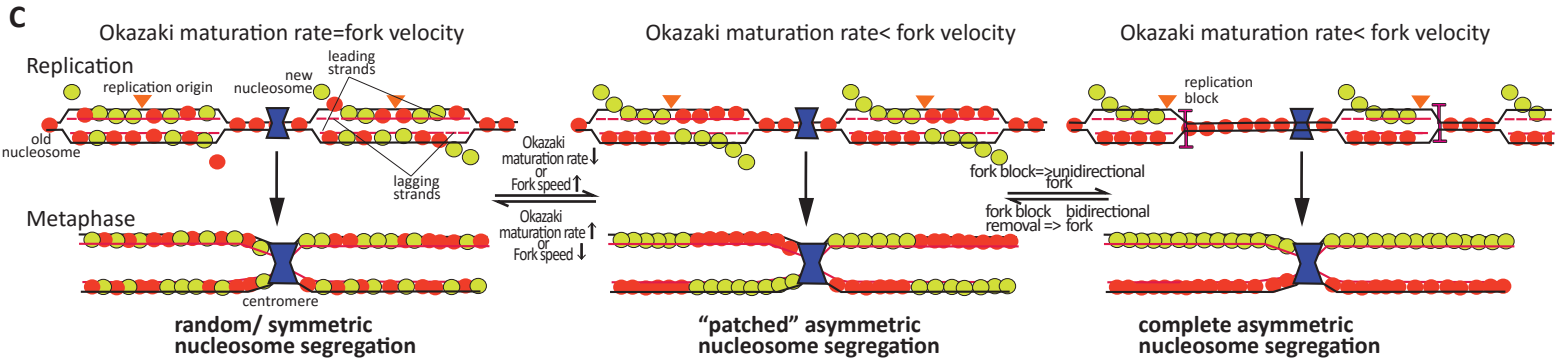

Figure 6

Supplementary Material

Table S1: Replication origins from Figure 1C
Table S2: Proposed ACS in Origins from Figure 1C
Table S3:Yeast Strains
Figures S1-S6

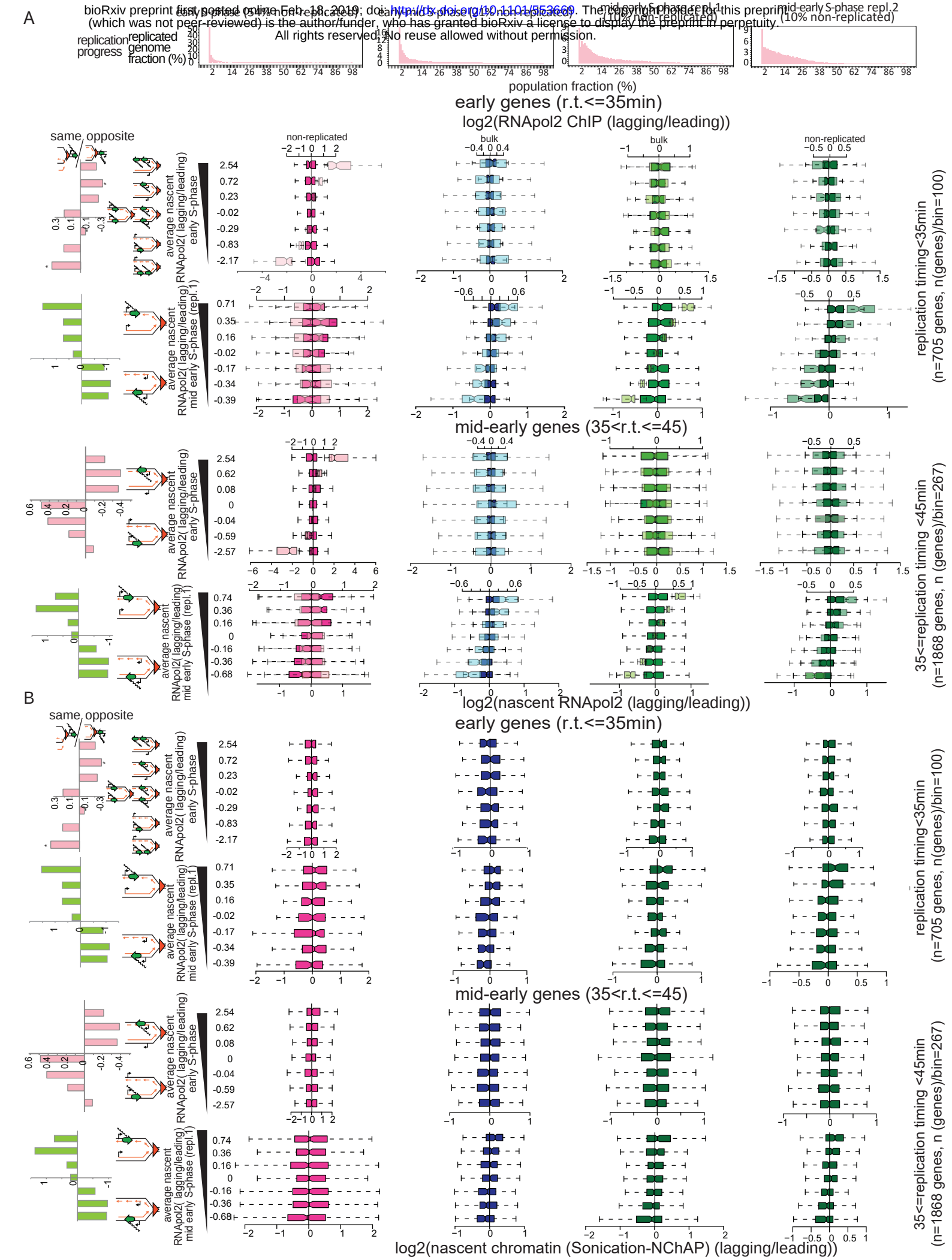

Supplementary Figure S1: Lagging and Leading strand read density distributions from ChIP (bulk and non-replicated) and NChAP (nascent chromatin) are symmetrical. A As in Figure 2D with log2 (RNApol2 ChIP (lagging/leading)) box plots in dark superimposed on log 2(nascent RNApol2-ChIP-NChAP(lagging/leading)) distributions in light boxes. **B** log2 (nascent chromatin (NChAP)(lagging/leading)) box plot

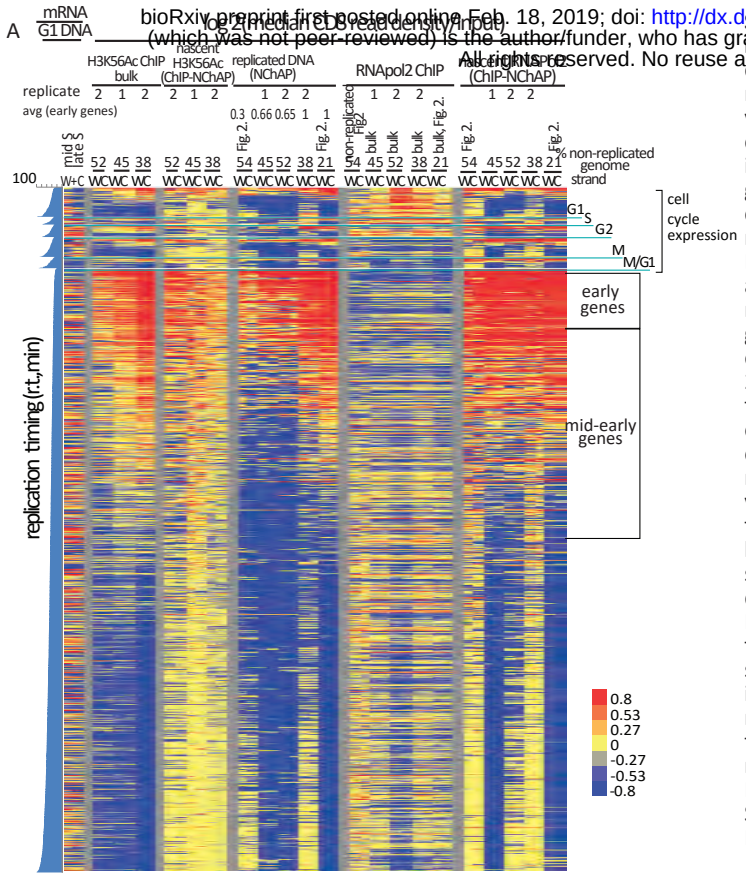

Supplementary Figure S2. Asymmetric distribution of RNApol2 and H3K56Ac on replicated gene copies replicate time-course in early S-phase. A. Replicate time course experiments in early S-phase were performed as outlined in Figure 1. The Heat map shows median RNApol2 and H3K56Ac occupancies in coding regions (CDS) of all yeast genes. H3K56Ac and RNApol2 ChIPs were performed in parallel from the same cell culture as indicated by the replicate number above the heat map. Each line is an individual gene and columns represent occupancy values for (W)atson and (C)rick gene copies for different S-phase time points : early S (45% non-replicated (time course 1), 52% and 38% replicated (time course 2)) from the ChIP, NChAP (sonicated nascent chromatin) and ChIP-NChAP (Nascent RNApol2 and H3K56Ac) fractions. Early-mid S (21% non-replicated) and early (54% non-replicated) datasets from Fig. 2 are added for comparison. The first two columns on the left represent mRNA enrichment over G1 genomic DNA in mid and late S (in the absence of EdU) determined with gene expression microarrays (Vasseur et al., 2016). Genes are grouped by cell cycle expression patterns and then ordered by replication timing within each group as in Fig. 2(replication timing determined in Vasseur et al., 2016). Median read density values for each gene have been normalized by separately dividing the W and C read densities of each gene in the ChIP and NChAP fractions with the W and C average read density of the sonicated input fraction for the same gene. The ChIP-NChAP medians have been normalized by dividing the W and C values with the input normalized W and C average values from the ChIP fraction. Due to the stochastic nature of replication origin activation it is impossible to precisely reproduce each early S-phase time point from one biological replicate to the other. Early S-phase time points were therefore further sorted according to replication progression by calculating the average median NChAP density of W and C reads for early genes (n=705), which shows that the replicate from Figure 2 (54% non-replicated) with an average NChAP read density of 0.3 is the earliest time point, followed by the 45% and the 52% non-replicated points, which are at the same stage in S-phase and finally with the 38% non-replicated time-point as the latest in early S. **B.** Box plot distributions of lagging/leading nascent RNA pol2 and H3K56Ac ratios from early to mid-early S-phase (columns left to right) for early genes (rows 2-4 from the top) (r.t.= replication timing). The top row shows the distribution of genome read densities (in 400bp bins) normalized to the maximum read density for each NChAP fraction (reads have not been normalized to input) at indicated time points in S-phase. The bar graphs on the left show the "same" gene enrichment calculated as in Fig. 2C for gene bins indicated in the Y axis of each row on the right.

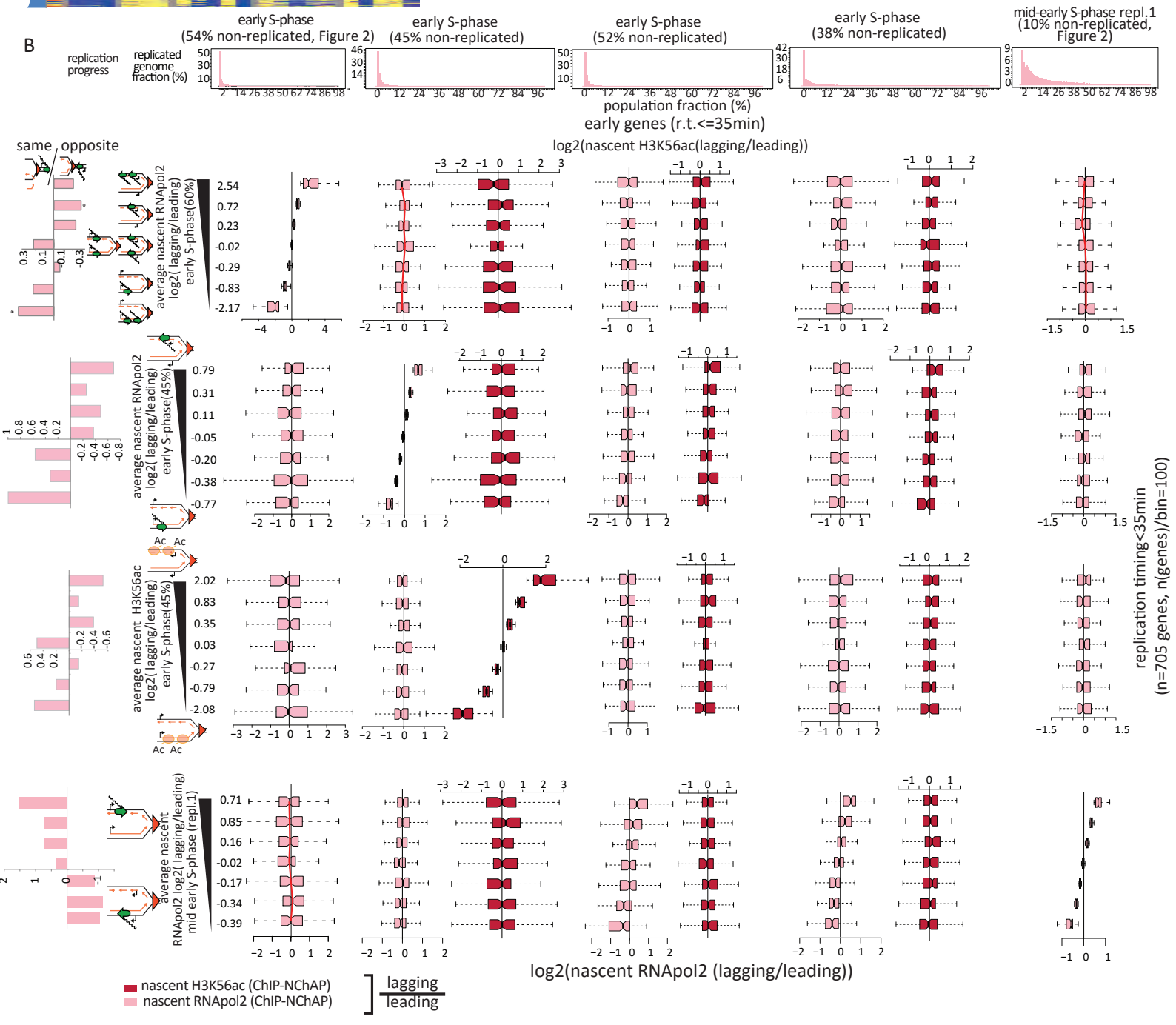

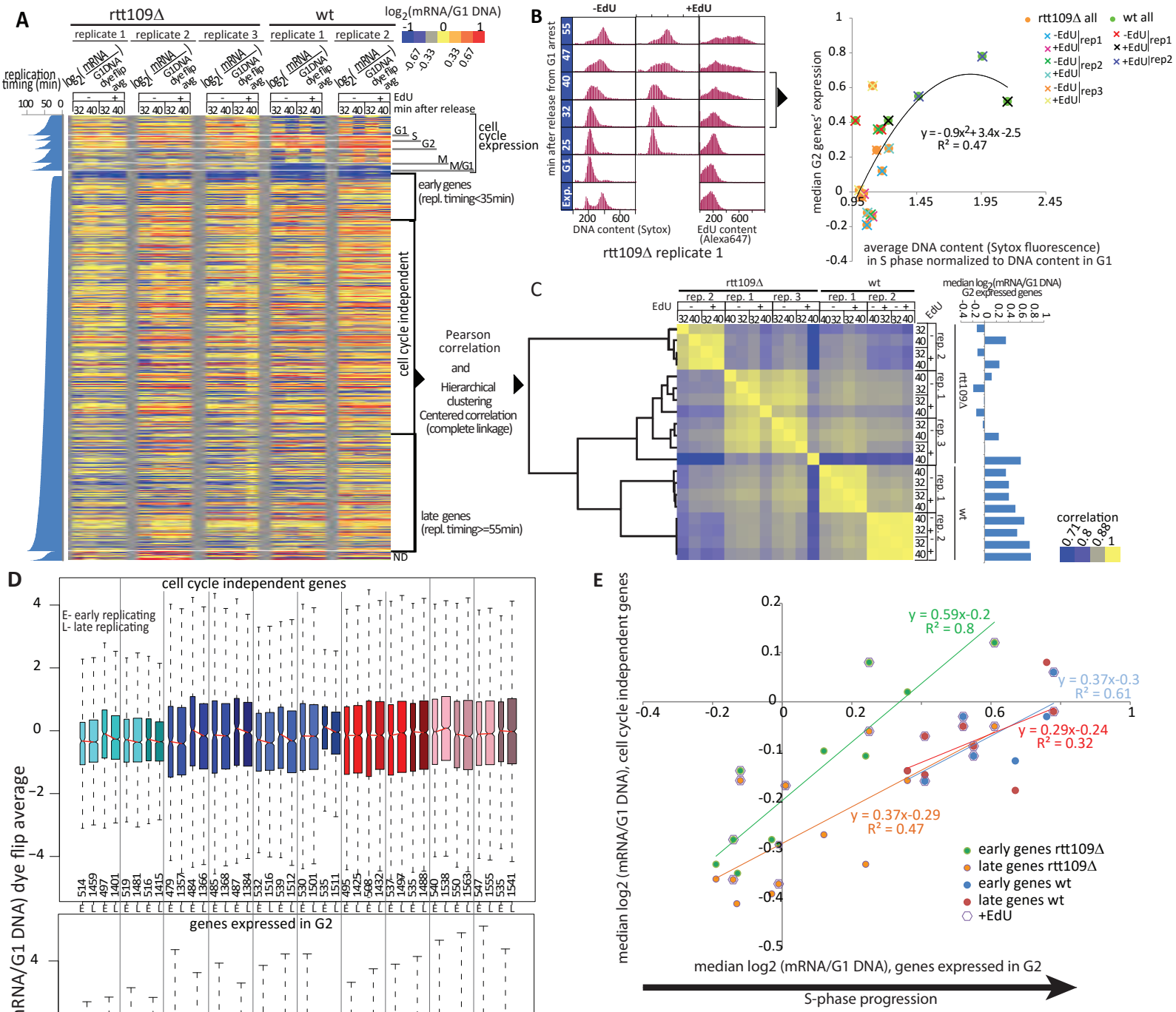

Supplementary Figure S3: Transcription buffering is reduced and EdU addition has no effect on gene expression in rtt109D cells. A.The heat map shows the results of gene expression two channel microarray (Agilent) experiments (three biological replicates for the rtt109 deletion mutant and two for wt (published in Vasseur et al, 2016, strain PV1). Each line represents average log2 ratios (two probes per gene) of mRNA 32min and 40min after release from G1 arrest (α factor) with or without EdU versus genomic DNA isolated from G1 arrested cells. Each value is an average of two dye flip technical replicates. All yeast genes are grouped by cell cycle expression and ordered by replication timing. Cell Cycle annotations were taken from the SGD database.**B.** Left: Cytometry analysis of DNA (labelled with Sytox) and EdU (Alexa647) content for the rtt109Δ replicate 1 in A. Right:Correlation of median G2 genes' expression (from A.) and average DNA content measured by Sytox fluorescence normalized to G1 DNA content for indicated rtt109Δ and wt samples (32 and 40 mins after release from arrest). Since rtt109Δ cells have a longer cell cycle and a longer S-phase, samples from rtt109Δ cells were fixed in earlier stages in S-phase than wt cells even though all replicates from both strains were crosslinked at the same time after release from arrest (32min or 40min). **C.** We determined pairwise Pearson correlations for cell cycle independent genes (4992 genes) in all samples and performed hierarchical clustering shown in the heat map. While gene expression levels are highly correlated among all samples (all correlations are 0.7 or higher), the highest similarity is observed between time points in the same biological replicate independently of EdU addition. rtt109Δ and wt time points cluster separately as well. Cell populations from different samples are at different stages of S-phase as shown in the bar graph of median expression of G2 specific genes on the right, which probably accounts for observed differences between time points and biological replicates. Expression of G2 genes is used as a measure of S-phase progression because they are directly correlated as shown in B. **D.** Box plot distributions of relative mRNA copy number for early and late replicating cell cycle independent genes (shown in A, Top), and G2 specific genes (Bottom, median mRNA levels are shown in red and medians for the 2nd and 3rd quartiles are in black on each box).**E.** Correlation of mRNA copy number and S-phase progression (measured by median G2 genes' expression from B-D) for early and late replicating genes (shown in A) from all rtt109Δ and wt samples. Transcription buffering is reduced in rtt109Δ cells since later in S-phase, early genes that have been replicated in most cells are more expressed than late genes that have not yet been replicated. Conversely, transcription is buffered after replication in wt cells since we observe no difference in early and late gene expression in wt cells.

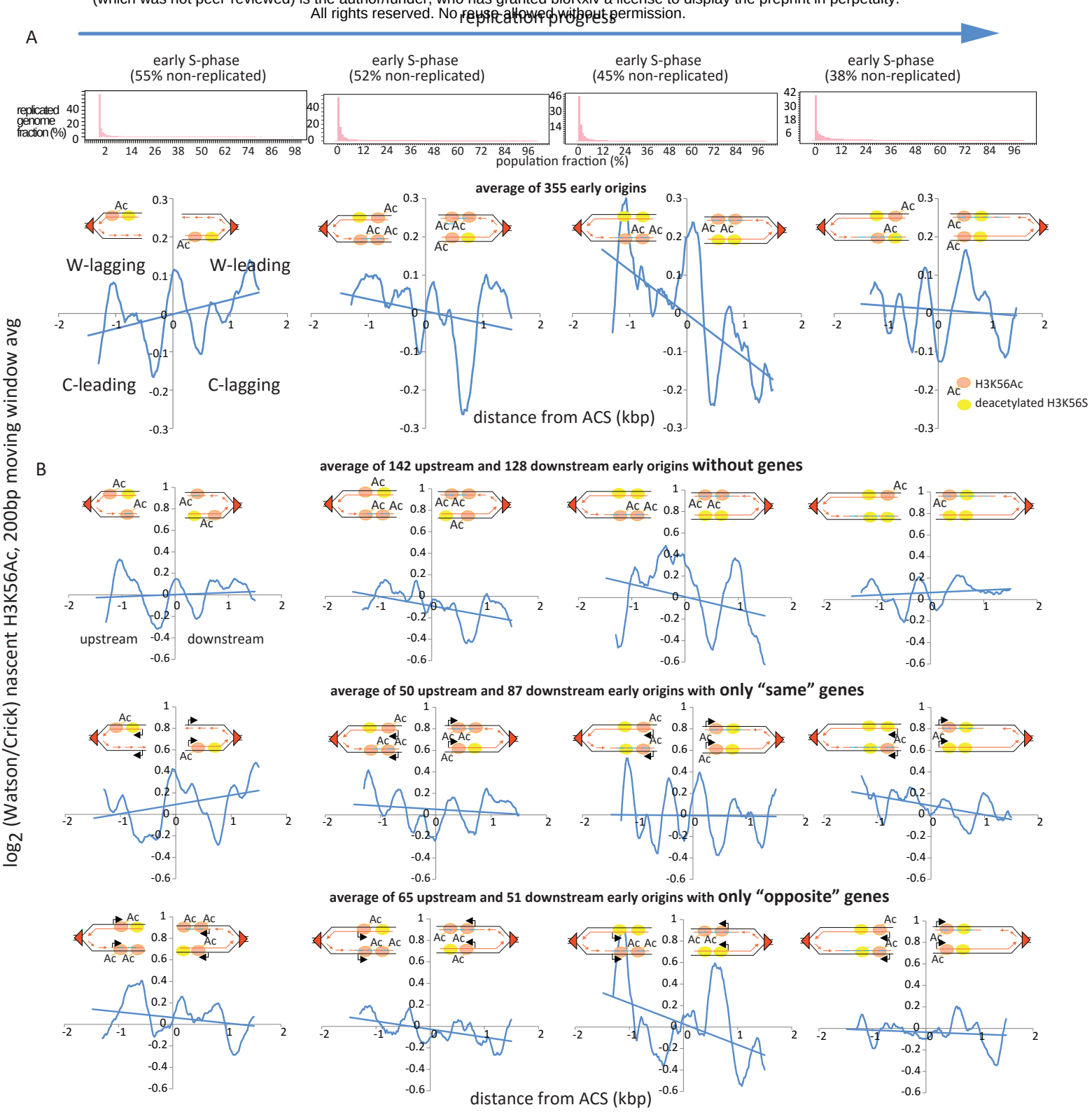

Figure S4: Early S-phase dynamics of H3K56Ac distribution on nascent chromatin 1500bp around early origins. A. Average read density ratio profiles between Watson and Crick reads 1500bp around ACSs of 355 early origins (replication timing below 35min, Table S1) from sonicated early S-phase H3K56Ac ChIP-NChAP datasets (Figure S2) show a shift from leading strand enrichment to lagging strand enrichment as replication progresses and chromatin matures. Read densities were only normalized to the average genome read density in each timepoint (Watson and Crick reads were treated separately), there was no input normalization for this analysis. We used the ACS consensus sequence (Nieduszynski et al., 2007) to find putative ACSs within ARS sequences identified in Figure 1 (Table S1). The identified putative ACS sequences are listed in Table S2. For origins with multiple ACS candidates only one of the ACS sequences (the one closest to the NChAP peak, Figure 1) was used for read density alignment. Time points are ordered by replication progression from earliest to latest as shown in the bar graphs in the top panel and described previously. The replication fork diagrams in each profile plot are a schematic interpretation of the observed H3K56Ac distribution. The H3K56 "deacetylated" nucleosome represents either a maternal "recycled" nucleosome or a new nucleosome in which the H3K56Ac has been removed by a deacetylase, the two being indistinguishable in our assay. **B.** The 355 origins from A were divided into three groups according to gene content: origins with upstream or downstream gene free 1500bp regions (top), with only "co-directional" genes (transcription and replication travel in the "same" direction)(middle) and with only counter-directional genes (transcription and replication travel in "opposite" directions) (bottom).

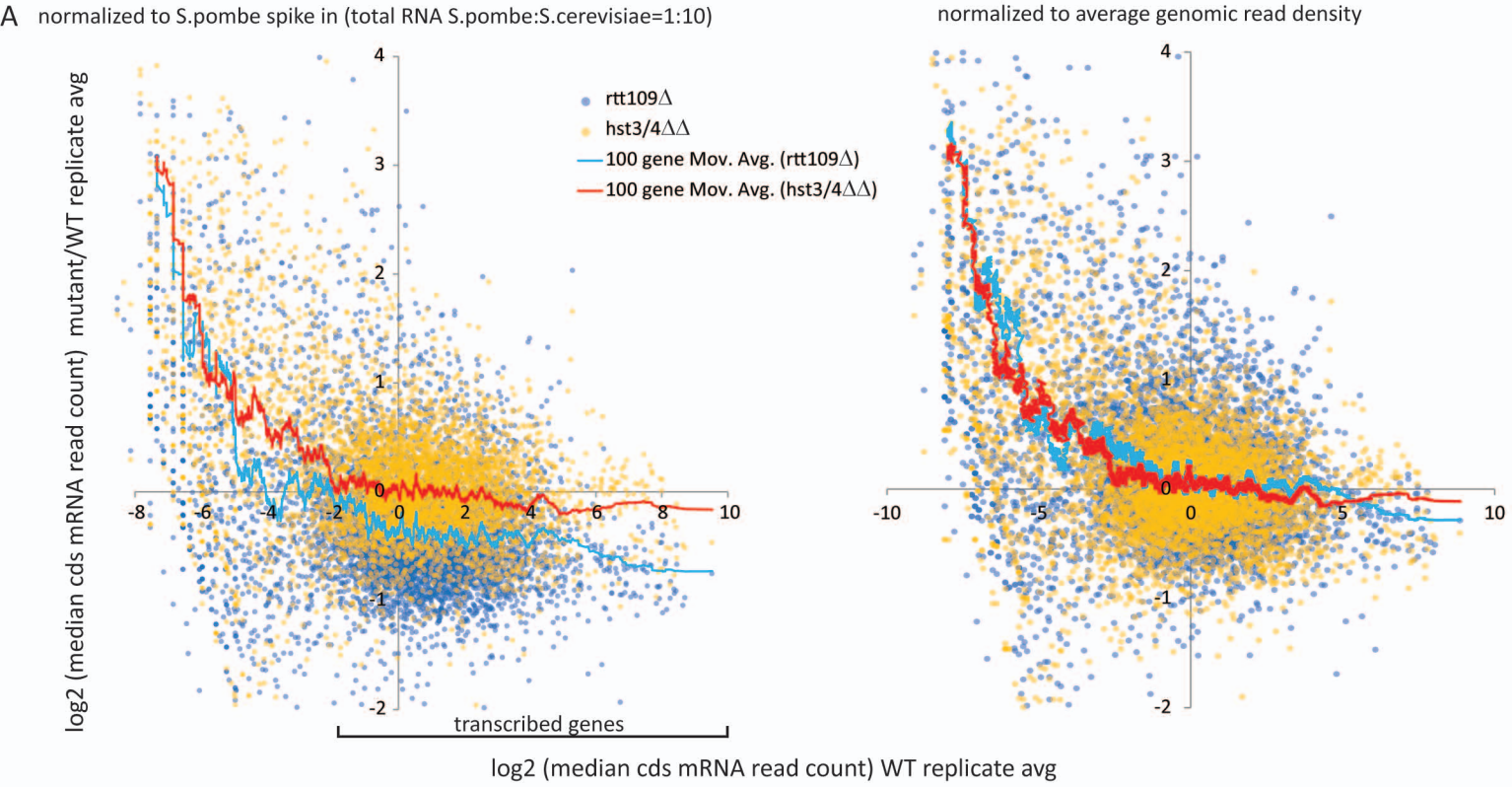

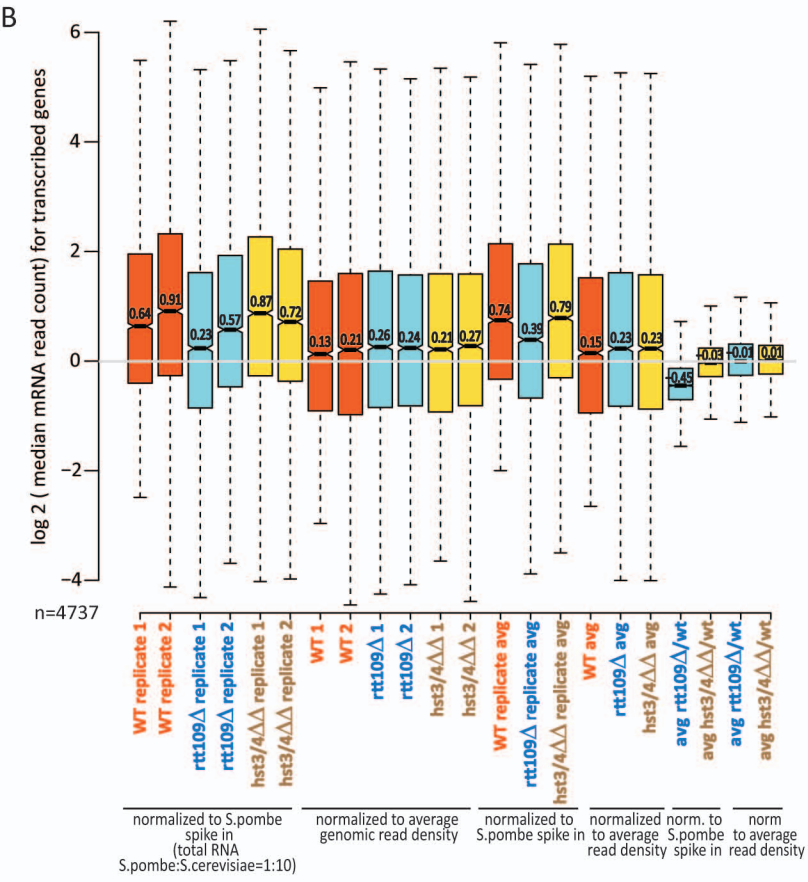

Figure S5: mRNA levels are globally reduced in the absence of H3K56ac. A. Total RNA was isolated from wt, rtt109Δ (H3K56 acetylase) and Hst3/4ΔΔ (H3K56 deacetylases) exponentially growing cells (2 replicates each). Total RNA from S.pombe was added to each sample in a 1:10 ratio. Strand specific high-throughput sequencing libraries were then made from isolated polyA RNA. S.Cerevisiae sequencing reads were normalized to the average genomic read density of the S.pombe spike in (left) or of the S.Cerevisiae sample (right). Median sense mRNA levels for each gene (introns were excluded from the calculation) were determined in all samples. The scatter plots show the ratio between mutant and wt mRNA levels for each gene relative to wt mRNA levels. Spike in normalization (left) reveals that mRNA levels in rtt109Δ cells are globally reduced compared to wt, while deletion of hst3 and 4 deactylases has no effect on steady state transcription output. Relative gene expression levels are not affected in either mutant as shown with the internally normalized datasets on the right. **B.** Box plot distributions of median mRNA levels per gene coding region for indicated datasets. Only transcribed genes (shown in A (left panel) were used for the analysis (4737 genes). The average median decrease in global mRNA levels in rtt109Δ cells relative to wt cells is ~30% ($1-2^{-0.45}$)

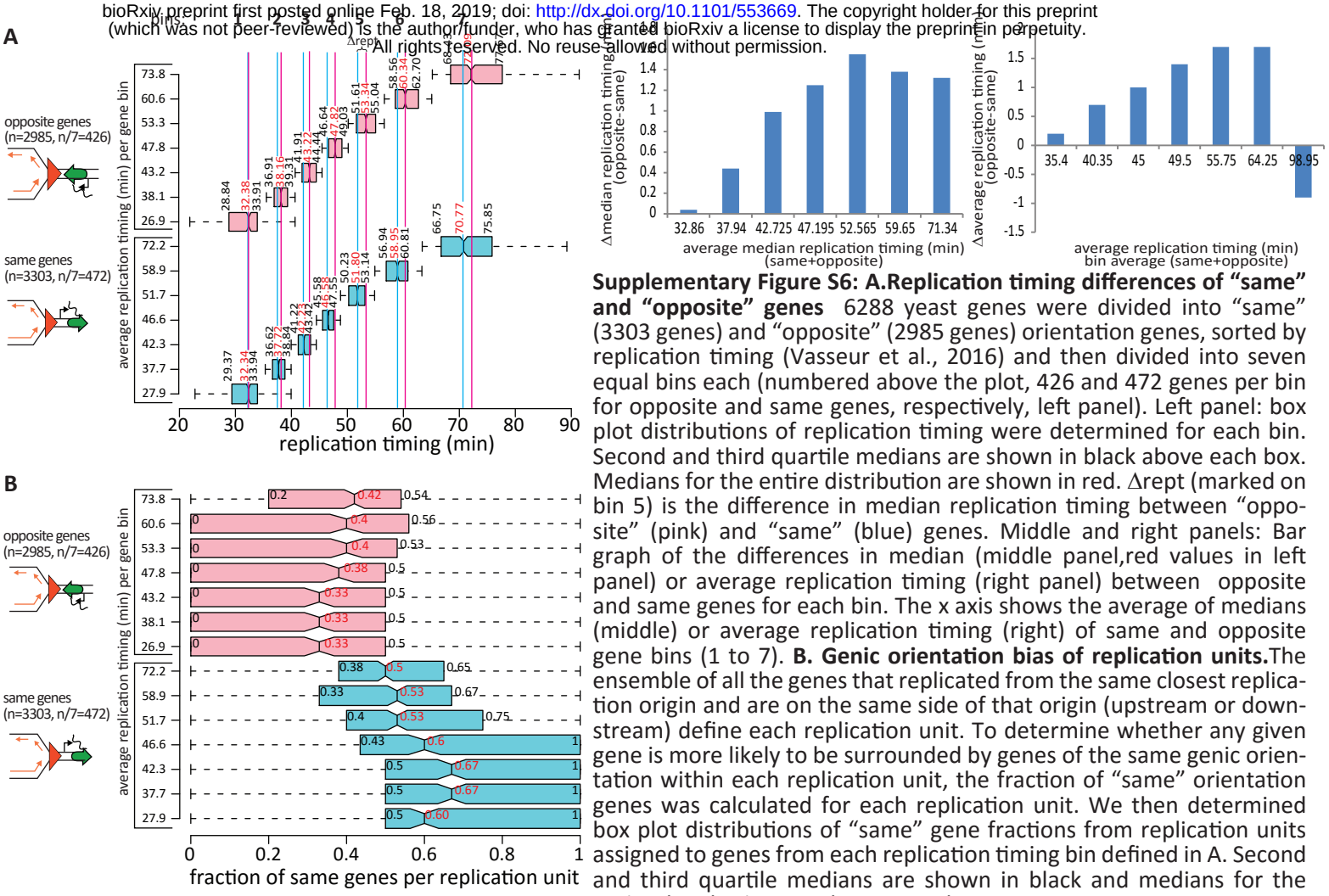

Supplementary Figure S6: A.Replication timing differences of "same" and "opposite" genes 6288 yeast genes were divided into "same" (3303 genes) and "opposite" (2985 genes) orientation genes, sorted by replication timing (Vasseur et al., 2016) and then divided into seven equal bins each (numbered above the plot, 426 and 472 genes per bin for opposite and same genes, respectively, left panel). Left panel: box plot distributions of replication timing were determined for each bin. Second and third quartile medians are shown in black above each box. Medians for the entire distribution are shown in red. Δrept (marked on bin 5) is the difference in median replication timing between "opposite" (pink) and "same" (blue) genes. Middle and right panels: Bar graph of the differences in median (middle panel,red values in left panel) or average replication timing (right panel) between opposite and same genes for each bin. The x axis shows the average of medians (middle) or average replication timing (right) of same and opposite gene bins (1 to 7). **B. Genic orientation bias of replication units.**The ensemble of all the genes that replicated from the same closest replication origin and are on the same side of that origin (upstream or downstream) define each replication unit. To determine whether any given gene is more likely to be surrounded by genes of the same genic orientation within each replication unit, the fraction of "same" orientation genes was calculated for each replication unit. We then determined box plot distributions of "same" gene fractions from replication units assigned to genes from each replication timing bin defined in A. Second and third quartile medians are shown in black and medians for the entire distribution are shown in red.